

# Space Vehicle Design Team

AOE 4165

---

## VT LUNA: C3 Cosmic Challenge

---

*"Autonomous Lunar Infrastructure Construction"*



**Submitted by:**

Eider Belda Cano    Jonah Bradley    Ty Brennan    Timothy Currey  
Katherine Evans    Duncan Foster    Nicholas Harvey    Robert Higinbotham  
Abinav Khadka    Braeden Peterson    Hugh Young III

**Faculty Advisor:**

Dr. Kevin Shinpaugh



**Kevin T. Crofton Department of  
Aerospace and Ocean Engineering**

Virginia Polytechnic Institute and State University  
1600 Innovation Drive, Room 241, Blacksburg, VA 24060

December 12, 2025

# Contents

List of Figures . . . . .	iv
List of Tables . . . . .	v
<b>1 Introduction</b>	<b>1</b>
1.1 Project Background . . . . .	1
1.2 Problem Definition . . . . .	2
1.2.1 Scope . . . . .	2
1.2.2 Stakeholders . . . . .	2
1.2.3 Timeframe . . . . .	3
1.3 Robotics's Griffin Lunar Lander . . . . .	3
1.3.1 Structure . . . . .	4
1.3.2 Propulsion System . . . . .	4
1.3.3 Guidance, Navigation, Control System . . . . .	4
1.3.4 Power System . . . . .	5
1.3.5 Avionics System . . . . .	5
1.3.6 Communications System . . . . .	5
1.3.7 Thermal Control System . . . . .	5
<b>2 Value System Design</b>	<b>6</b>
2.1 Introduction . . . . .	6
2.2 Mission Objectives . . . . .	7
2.2.1 Scalability . . . . .	7
2.2.2 Impact . . . . .	7
2.2.3 Time . . . . .	7
2.2.4 Risk . . . . .	7
2.2.5 Cost . . . . .	7
2.2.6 Mission Performance Ranking . . . . .	7
<b>3 Mission Overview</b>	<b>9</b>
3.1 Objectives . . . . .	9
3.1.1 Key Requirements . . . . .	9
3.1.2 Key Mission Elements . . . . .	10
3.2 Concept of Operations (CONOPS) . . . . .	10
3.3 Fabrication Trade Study . . . . .	11
<b>4 Landing Site Selection</b>	<b>13</b>
4.1 Lunar Regolith . . . . .	16
4.1.1 Lunar Topography . . . . .	17

4.1.2	Regolith Chemical Makeup . . . . .	18
4.1.3	Regolith Sintering . . . . .	18
<b>5</b>	<b>System Synthesis</b>	<b>21</b>
5.1	Regolith Tile Properties . . . . .	21
5.1.1	Material Properties . . . . .	21
5.1.2	Design Properties . . . . .	25
5.2	Sintering Model . . . . .	27
5.2.1	Justification . . . . .	27
5.2.2	Method . . . . .	28
5.2.3	Results . . . . .	29
5.3	General Architecture Trade Study . . . . .	30
5.3.1	Independent Rover . . . . .	30
5.3.2	Umbilical Cord . . . . .	31
5.3.3	Dock to Charge . . . . .	31
5.3.4	Stationary Tile Maker . . . . .	32
5.3.5	Final Choice . . . . .	33
5.4	Regolith Collection System (Rover) . . . . .	33
5.4.1	Excavator Arm Design . . . . .	34
5.4.2	Tires and Mobility System . . . . .	35
5.4.3	Navigation System . . . . .	35
5.4.4	Hopper and Storage . . . . .	36
5.4.5	Power System . . . . .	37
5.4.6	Computer systems . . . . .	38
5.4.7	Structural Frame and Chassis Design . . . . .	39
5.4.8	Thermal Management and Heating System . . . . .	39
5.4.9	Summary . . . . .	39
5.5	Manufacturing System (Stationary Tile Maker) . . . . .	40
5.5.1	Collection . . . . .	40
5.5.2	Conditioning . . . . .	40
5.5.3	Microwave Sintering . . . . .	42
5.5.4	Cooling Subsystem Architecture . . . . .	43
5.6	Communication System . . . . .	45
5.6.1	Griffin Lunar Lander Communication System . . . . .	45
5.6.2	Rover Communication System . . . . .	47
<b>6</b>	<b>Architecture Analysis</b>	<b>50</b>
6.1	Mass Budget . . . . .	50
6.2	Power Budget . . . . .	52
6.3	Cost Analysis . . . . .	53
6.4	Risk Analysis . . . . .	54
6.5	Future Work . . . . .	56
6.5.1	Rover Autonomy and Terra-forming . . . . .	56
6.5.2	Tile Testing . . . . .	56
6.5.3	Finite Element Analysis . . . . .	57
6.5.4	Interlocking Tile Designs . . . . .	57

6.6 Conclusion . . . . .	59
--------------------------	----

<b>References</b>	<b>60</b>
-------------------	-----------

# List of Figures

1	Astrobotic's Griffin Lunar Lander [9]. . . . .	3
2	Diagram of Griffin's Propulsion System [9]. . . . .	4
3	System Flow Chart showing the categories and subcategories of the value system design. . . . .	6
4	Concept of Operations for the mission. . . . .	10
5	Lunar South pole solar illumination yearly average showing craters with low to no illumination and areas of high illumination on crater rims [12]. . . . .	13
6	Shackleton crater yearly average illumination further illustrating the differences in illumination throughout a crater at this potential landing site [12]. . . . .	14
7	NASA's 13 candidate landing regions for Artemis III [13]. . . . .	15
8	NASA's redefined candidate landing regions for Artemis III [14]. . . . .	15
9	Topographical map of the Moon detailing average altitude deviation [16]. . . . .	17
10	Void holes in sintered products [17]. . . . .	18
11	Visual representation of problems with sintering particles such as shrinkage and bubbling [19]. . . . .	19
12	Sintering speed of lunar regolith simulant under microwave heating [22]. . . . .	20
13	A graph detailing the relationship between compressive strength and porosity [26]. . . . .	22
14	Graphs with relationships between sintering temperature density, shrinkage, and porosity [28]. . . . .	23
15	A graph detailing the relationship between highland sintering temperature and density [29]. . . . .	24
16	A graph detailing the relationship between mare sintering temperature and density [29]. . . . .	24
17	A graph detailing the relationship between regolith density and compressive strength [29]. . . . .	25
18	Image of the tile design, a normal hexagon with a circumscribed radius of 0.15 m, a depth of 0.106 m, and a 25 mm fillet. . . . .	26
19	Model figure graphing the total time to sinter one tile against the Applicator area that resulted in that time, the trough shows the optimal applicator area . . . . .	29
20	Diagram of the Griffin lunar lander highlighting high and medium gain antennas which allow the lander to communicate to Earth in the X-band [9]. . . . .	46
21	Diagram of communication process between rover, lander, and ground station [9]. . . . .	47
22	Depiction of the range for antennas based on their dBi (low gain 0 - 3 dBi, medium gain 3 - 8 dBi, high gain 9 - 15 dBi) [102]. . . . .	48
23	Risk Matrix detailing the likelihood and consequence of failure before and after mitigation. . . . .	56
24	Image of the dovetailed tile design highlighting how the tiles interlock with each other to transfer loads. . . . .	58
25	Technical drawing of the vertically interlocking tile design showing that a lack of vertical homogeneity allows for tiles to interface with each other in the out of plane dimension [32]. . . . .	59

# List of Tables

1	Weighted Ranking of Evaluation Criteria. . . . .	8
2	System Requirements: Displays the Requirements of the System. . . . .	9
3	Fabrication Method Trade Study Summary. . . . .	12
4	Lunar Regolith Compound Concentration [15]. . . . .	16
5	Lunar Regolith Compound Concentrations by Mare[15]. . . . .	18
6	Boiling Points and Vacuum Sublimation Temperatures of Lunar-Relevant Oxides [20]. . . . .	19
7	Regolith Tile Requirements: This table displays the requirements of the regolith tiles. . . . .	21
8	Loading Conditions Experienced by Landing Pad During a Simulated Landing [25]. . . . .	22
9	Material Properties of Sintered Lunar Regolith Simulant Samples by Temperature [27]. . . . .	23
10	Required Nomenclature for the Model Equations.[33][34][35][36] . . . . .	27
11	Core Modeling Equations Required to Relate the Sintering Process to Lunar Regolith Material Properties.[34][33]	28
12	Strengths and Weaknesses of the Independent Rover Architecture. . . . .	30
13	Strengths and Weaknesses of the Umbilical Cord Architecture. . . . .	31
14	Strengths and Weaknesses of the Dock to Charge Rover Architecture. . . . .	32
15	Strengths and Weaknesses of the Stationary Tile Maker Architecture. . . . .	32
16	Rover Arm Segment Properties and Torque Influence. . . . .	34
17	Torque Requirements and Motor/Gearbox Selection for Rover Arm Joints. . . . .	34
18	Rover Subsystem Peak Power Consumption. . . . .	38
19	Rover Computing Subsystems, Responsibilities, and Mass Estimates. . . . .	38
20	Vibratory Sifter Motor Specifications. . . . .	41
21	Trade Study Comparison of Potential Cooling Architectures for Regolith Tile Manufacturing [93].	43
22	Mass Budget with Growth Allowance. . . . .	50
23	Table 22 Continued. . . . .	51
24	Power Draw by Operating Mode for Stationary Tile Factory. . . . .	52
25	Rover Power Usage Summary. . . . .	52
26	Subsystem and Component Cost Estimates for Rover & Tile Maker. . . . .	53
27	Risk Level Definition. . . . .	54
28	Risk Classification Legend. . . . .	54
29	High Level Mission Risks and Mitigation Outcomes. . . . .	55

# 1 Introduction

## 1.1 Project Background

NASA's Artemis program is spearheading the effort to bring humanity back to the moon, this time to establish a permanent foothold and create a sustainable, lasting human presence on the lunar surface.

Artemis I, launched in 2022, provided the first full-system test of the Space Launch System (SLS) and Orion crew vehicle in a cislunar environment, validating critical guidance, navigation, propulsion, and thermal-protection systems. Artemis II, scheduled to launch in February of 2026, will be the first crewed flight of NASA's SLS rocket and the Orion spacecraft, marking humanity's return to lunar vicinity flight since Apollo 17. With a mission duration of about ten days, it will carry four astronauts on a free-return trajectory around the Moon, meaning Orion uses Earth and lunar gravity to loop the Moon and return home without major propulsion after the initial burn [1].

Artemis III plans to deliver astronauts to the lunar surface. This will be the first crewed lunar landing since 1972, targeting exploration of the lunar South Pole region. This mission moves beyond orbital operations to surface access by integrating NASA's Orion spacecraft with a commercial Human Landing System (HLS), currently being developed with SpaceX's Starship variant. The mission emphasizes scientific investigation of polar geology, volatiles, like water and ice, and surface processes that are critical for understanding the Moon's history and supporting future long-duration missions. Artemis III will also test advanced spacesuits and surface mobility concepts [1]. Artemis IV is the first mission planned to interact with NASA's "Gateway", a small lunar orbiting outpost being built in partnership with international space agencies. Scheduled for September of 2028, Artemis IV will deliver the Lunar I-Hab module to Gateway and support additional lunar surface visits. This mission begins the creation of a sustained lunar orbital infrastructure, improving access, flexibility, and science return for surface missions while serving as a testbed for technologies needed for Mars exploration. During these missions, most notably Artemis III and IV, a crew will be deployed, exploring the south pole region of the moon and debuting the first lunar space station [1]. To achieve this level of sustained presence on the harsh environment that is the lunar surface, extensive infrastructure is required. This is where COSMIC and its challenge steps in.

In 2022, the White House released a national strategy for the advancement of In-Space Assembly and Manufacturing (ISAM) capabilities. The strategy outlined six general steps to advance and prioritize ISAM development. As a response, the Consortium for Space Mobility and ISAM Capabilities (COSMIC) was created. COSMIC acts as a hub for over 250 organizations, including but not limited to: federal agencies, universities, research institutes, and commercial companies, to assess ISAM needs and advance its prerogative [2]. In their newest challenge, the C3 COSMIC Capstone Challenge, COSMIC invites students to develop conceptual missions and designs for spacecraft operations in-orbit or on the lunar surface [3].

The VT LUNA team has elected to participate in Track 2 of this capstone challenge: C3-Lunar, with problem statement as follows: Design a payload, to be delivered by the Griffin lunar lander, that can create infrastructure for a permanent lunar outpost [3].

Given this challenge, the goal of VT LUNA is to design an autonomous system capable of constructing lunar

infrastructure, specifically lunar landing pad tiles, using In-Situ Resource Utilization (ISRU) techniques. The mission timeline targets a launch in the late 2020s or early 2030s, aligning with the Artemis program support window.

## 1.2 Problem Definition

### 1.2.1 Scope

Currently, there is no established lunar base or any accompanying infrastructure, and there are many such examples of infrastructure to choose from this blank slate. With a problem statement as general as 'create infrastructure for a permanent lunar outpost,' one might wonder how VT LUNA arrived at the conclusion of constructing lunar landing pads. The first step in creating a lunar outpost is the consistent delivery of Earth technologies and payloads. To deliver logistical equipment, build surface assets, and rotate crew members, numerous landings and launches are required on the lunar surface. These launches and landings must be safe, reliable, and within a relative range of the established outpost.

Lunar regolith, or moon dust, poses a great risk to the launch/landing requirements, as well as the safety of other previously delivered Earth technologies. Lunar regolith is extremely fine, abrasive, and electrostatically active, with a study done by NASA concluding that the regolith is a "significant and pervasive risk [4]." When a lander fires near the surface of the moon, it erodes the loose regolith beneath it and accelerates the particles to velocities up to  $2 \text{ km/s}$ , a speed high enough to sandblast and damage hardware even kilometers away [5]. This uncontrolled erosion or plume ejecta can also crater and destabilize the landing zone for vehicles and even threaten the lander's own structures and sensors.

This is where lunar landing pads become essential first-order infrastructure. Lunar landing pads replace loose, erodible regolith with a consolidated surface capable of withstanding the force of a rocket engine. With the addition of lunar landing pads, all other infrastructure is protected. They remove erosion and cratering under the vehicle, minimizing the threat to the landing system. They also prevent the high-velocity plume ejecta that poses a risk to other existing infrastructure, such as power systems, habitats, rovers, or other science payloads. In addition to mitigating regolith-related mission risks, the landing pads also provide a central delivery zone, enabling repeated, closely spaced landings. This allows the aforementioned delivery process to be streamlined and local, eliminating the need to venture in a rover to a distant landing point for earth shipments whenever a landing occurs. This aspect significantly decreases the overhead costs of missions and creates a more efficient environment for the astronauts to live and work in. VT LUNA is not alone in its conclusion on the importance of lunar landing pads as a necessary first step. NASA's Lunar Surface Innovation Initiative has identified landing and launch pads as a key infrastructure alongside ISRU and power [6].

Lunar dust and surface stability present significant hazards for repeated lunar landings. To support sustained lunar presence, landing pads are required to mitigate plume effects and provide stable landing zones. The system must operate autonomously to collect regolith, process it, and manufacture dense, durable tiles using microwave sintering.

### 1.2.2 Stakeholders

NASA's Artemis program represents the United States' next major initiative in human exploration, aiming to establish a sustainable human presence on the lunar surface and prepare for eventual crewed missions to Mars. Building upon the technological heritage of Apollo, the Space Shuttle, and the International Space Station, Artemis integrates new launch systems, spacecraft, landing architectures, and commercial partnerships to advance deep-space capability. The program's overarching objectives include returning astronauts to the lunar surface, developing the Lunar Gateway as an orbital staging platform, conducting high-value scientific

investigations of the Moon’s south polar region, and maturing surface infrastructure that enables recurring missions. If VT LUNA’s design were to lose the support from NASA’s Artemis program, then the concept of design proposed in this paper would have to be sold to another program, either international or local programs.

### 1.2.3 Timeframe

VT LUNA’s mission will likely launch in the late 2020s or potentially the very early 2030s in order to be in accordance with NASA’s lunar architecture timeline. The Artemis program is scheduled to send preliminary missions to the lunar surface in the late 2020s and will be followed by many more missions in the 2030s [7]. Landing pads are a critical piece of initial infrastructure, as they help ensure safer and less damaging landings on the surface, and thus will likely be constructed in the early 2030s. As the mission is a proof of concept, it will predate this construction period and therefore occur in the late 2020s. In this time frame, it is expected that the mission will have access to very little lunar architecture, as it is among the first pieces of infrastructure to be constructed. A key piece of infrastructure in landing pad construction could be water extraction architecture, as water can act as a binder; however, this technology is unlikely to be operational before the early 2030s to mid-2030s and thus cannot be assumed for the mission. Some assumptions that can be made include a 5 kW solar power supply from the Griffin lunar lander, as well as a local on-surface astronaut for tile relocation and testing. These assumptions are provided by COSMIC, the overseeing consortium of this project.

## 1.3 Robotics’s Griffin Lunar Lander

Astrobootic’s Griffin lander is a next-generation, medium-class lunar lander engineered to support missions requiring large payloads, precision landing, and extended surface operations in harsh polar environments. The Griffin lander is arranged, augmented, and adapted to the various payload delivery locations. However, Griffin is sized to accommodate a larger class of payload [8]. This flexibility allows Griffin to accommodate a variety of payload types for science, exploration, marketing, resources, and commemoration.

The Griffin design leverages a common Astrobootic spacecraft bus architecture that ensures subsystem reliability, modularity, and mission heritage. Griffin incorporates upgraded power, thermal, propulsion, and structural capabilities to meet the demanding operational requirements of polar and precision landing missions.

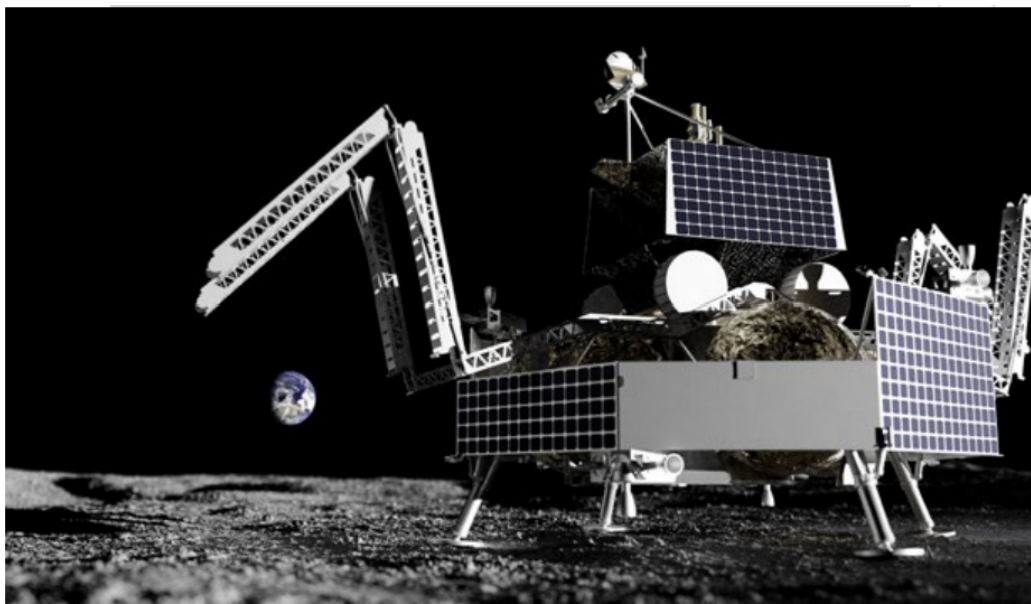


Figure 1: Astrobootic’s Griffin Lunar Lander [9].

### 1.3.1 Structure

The Griffin Lunar Lander has a strong and lightweight structure, allowing for increased survivability during landing and launching. The main structure is made up of an aluminum alloy and has three main components: the launch vehicle adapter cone, deck panels, and radiator panels for mounting payloads and avionics [8]. For missions to the surface of the Moon, the lander has four legs, designed to absorb the shock of landing and stabilize the craft.

Griffin consists of six major subsystems, including propulsion, guidance, navigation, and control (GNC), power, avionics, communications, and thermal control.

### 1.3.2 Propulsion System

The propulsion system is equipped with five 700 lbf pulsed main engines and twelve 25 lbf Attitude Control System (ACS) engines powered by pressure-fed propellant, which does not require ignition due to the fuel and oxidizer combusting on contact. Pulsed engines generate thrust through rapidly repeating combustion cycles. This offers a simpler design with fewer moving parts. The ACS engines are smaller thrusters on the lander that help with controlling the pitch, roll, and yaw of the spacecraft. This allows the lander to perform precise maneuvers like docking and landing on hazardous surfaces [9].

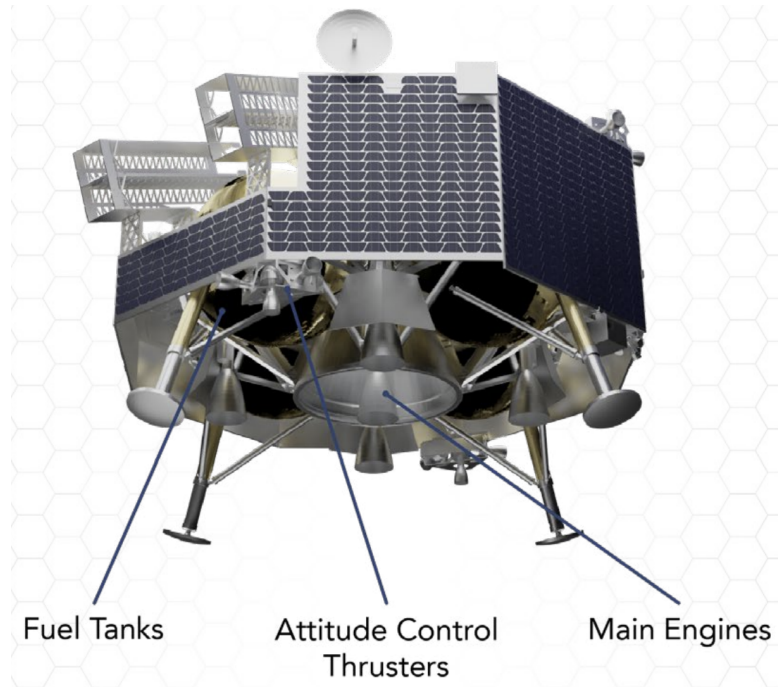


Figure 2: Diagram of Griffin’s Propulsion System [9].

### 1.3.3 Guidance, Navigation, Control System

The GNC system processes the inputs from an array of sensors, correcting for idiosyncrasies, and uses them to revise the internal estimate of the lander’s position, attitude, and velocity during flight. Commands to maneuver the lander are updated based on this estimate of the spacecraft’s state. Earth-based ranging informs position and velocity state estimates for orbital and trajectory correction maneuvers. Making use of a star tracker and sun sensors, the GNC system is able to orient the lander to constantly have its solar panels facing the Sun during cruise operations. During the landing sequence, a Doppler LiDAR provides the lander with range and range rate information that helps guide the lander to a safe landing at the target site [9].

Integrated into the GNC system are experimental Optical Precision Autonomous Landing (OPAL) sensors. These OPAL sensors are an advanced imaging-based terrain navigation package that consists of a camera and computer. The sensors use maps stored in the lander's memory and real-time images from the camera to estimate how the lander will land on the surface.

#### **1.3.4 Power System**

The Griffin Lunar Lander's power system is designed to be power positive, meaning it generates more power than it uses for all phases of flight besides the descent phase. The power system is also responsible for power storage, generation, distribution, and power management. On board, a panel of GaInP/GaAs/Ge triple junction solar cells with heritage in orbital and deep space missions generates the lander's power. The Griffin stores its power in a space-grade lithium-ion battery, which then feeds into a 28 Vdc power rail where the power is distributed to all of the lander's subsystems and even its payloads [9]. As stated, when outlining the GNC system of the lander, the Griffin lander's solar panels are consistently pointed towards the sun to maximize the amount of solar energy generated. After descending to the surface of the Moon, the power system continues to generate power reliably in order to service the lander and its payloads.

#### **1.3.5 Avionics System**

The avionics on board perform all command and data handling, managing the multiple different inputs and outputs of the lander's subsystems. On board, the Griffin Lunar Lander has an Integrated Avionics Unit (IAU) that houses ten boards, each with distinct functions that seamlessly help aspects of the avionics system and flight computer. The Griffin's flight computer consists of a 32-bit high-performance dual-core LEAON 3 FT microprocessor. To stay protected, the computer is equipped with radiation-hardened circuits, fault-tolerant and single-event upset (SEU) -proof characteristics. Also encompassed within the IAU is the payload computer. This computer monitors payload power consumption and directly communicates with the payloads [9]. Data and commands from the payload ground software are sent to the payload via the payload computer, and payload telemetry is packaged for downlink to Earth.

#### **1.3.6 Communications System**

Griffin's communications system provides the lander commands and telemetry. The communication system on board relays data between the payload customer and the payload. It is equipped with a high-powered transponder in order to communicate with Earth. The lander's connection to Earth uses different frequencies within the X-Band range for space communications. The lander is also equipped with multiple low-gain antennas for more optimized coverage when the lander is in cruise and when it is in lunar orbit operations. It then switches to its medium gain or its high gain antenna after it has touched down on the lunar surface, for increased bandwidth. Following landing, a 2.4 GHz IEEE 802.11n compliant Wireless Local Area Network (WLAN) modem enables wireless communication between the lander and deployed payloads on the lunar surface [9]. More information and its relevance about the communications system is provided in subsection 5.6.1.

#### **1.3.7 Thermal Control System**

Finally, the Griffin Lander's thermal control system is designed to have passive methods for thermal regulation. Radiators are on board to get rid of excess heat and radiate it out into space. Then, heat pipes are used to send excess heat to colder regions of the lander, wherever the excess heat is needed. To protect other components from undesired thermal effects, multi-layered insulation is used.

For the specific mission, the Griffin Lunar Lander offers a great amount of flexibility and customization.

## 2 Value System Design

### 2.1 Introduction

The most effective approach to identifying an optimal mission design is through the application of systems engineering principles. The Value System Design (VSD) helps outline which factors make one design more favorable than another and how these factors are weighted. The factors are weighted against each other using either qualitative or quantitative data. After analyzing the values of each factor, all potential mission architectures are evaluated. In this case, the results help determine the optimal configuration for the payload to construct lunar landing pads. The requirements that define mission success are used to establish the specific figures of merit for the study. Each of the proposed concepts will be systematically assessed against these weighted factors. The goal of this analysis is to produce a clear, justifiable recommendation on the most viable architecture to pursue for the next phase of design and development.

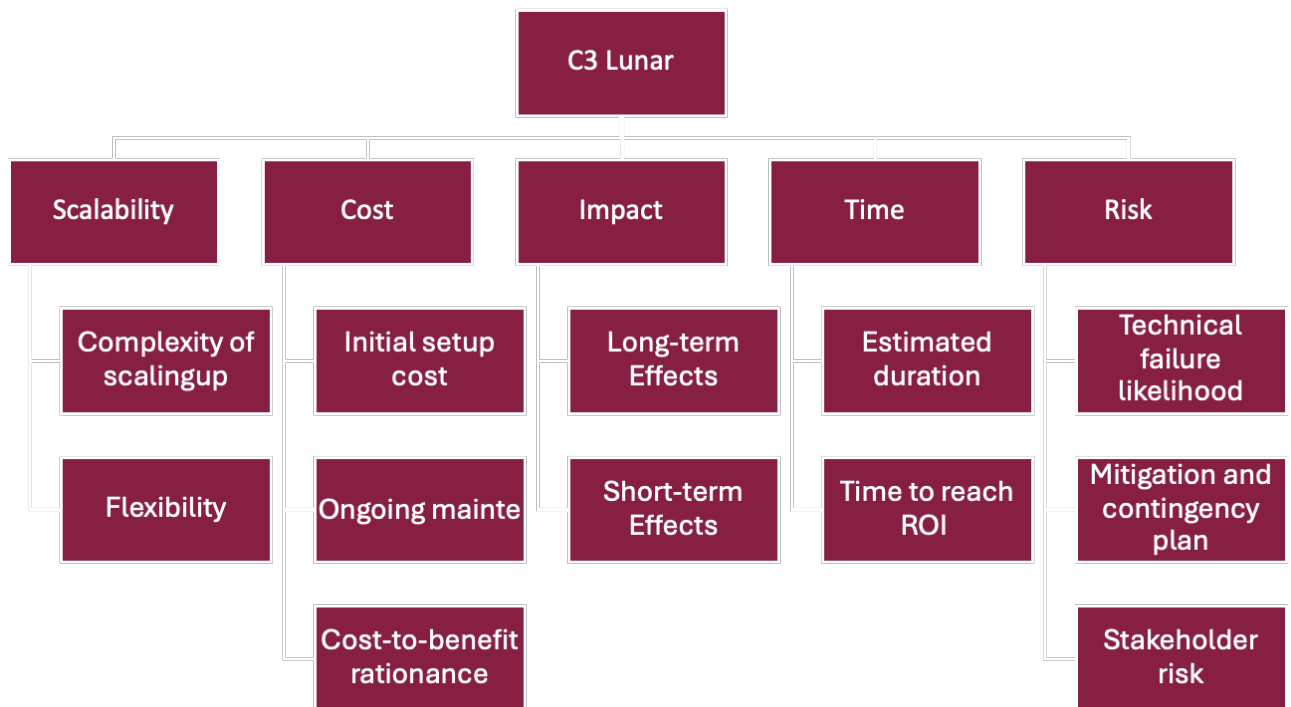


Figure 3: System Flow Chart showing the categories and subcategories of the value system design.

## 2.2 Mission Objectives

### 2.2.1 Scalability

This factor measures the potential for the design to be replicated, adapted, and expanded for full-scale infrastructure creation. The payload operates under strict weight and volume constraints. It cannot build a complete lunar base in a single mission; rather, it must demonstrate a viable method that can be scaled up. Therefore, the architecture must prove that the sintering and construction process is not limited to a small sample size but can be expanded to create large-scale landing zones. If the design cannot be scaled, the payload fails to demonstrate long-term utility.

### 2.2.2 Impact

Secondly, impact quantifies the importance and effectiveness of the mission beyond its initial success. This factor ensures that the purpose and significance of the mission justify the resource investment. High-impact missions secure support from potential stakeholders (such as NASA and commercial partners) by advancing the end goal of permanent lunar settlement. A mission with low impact implies that even if technical success is achieved, it does not meaningfully advance the state of the art or solve the critical problem of lunar dust mitigation.

### 2.2.3 Time

Next, time is a critical criterion driven by funding cycles and planning logistics. This metric evaluates the mission timeline from development to operational capability. Missions with extended timelines, or those requiring upwards of a decade to achieve a minor goal, face significant risks regarding funding continuity. Furthermore, the timeline is constrained by the interdependence of other lunar assets; for example, if the mission relies on equipment that has not yet arrived on the Moon, the timeline is compromised. Therefore, minimizing the time to mission completion is favorable.

### 2.2.4 Risk

Risk determines the probability of mission failure and the effectiveness of mitigation strategies. Since the C3 Lunar mission focuses on robotic infrastructure construction rather than human-manned missions, a higher tolerance of risk is accepted compared to crewed standards. However, risk remains a factor regarding the safety of the lander, the prevention of collisions with orbital debris, and the reliability of the payload after the shocks of landing. The design must ensure that the equipment operates correctly in the harsh lunar environment (vacuum and thermal extremes) to prevent total mission failure.

### 2.2.5 Cost

Cost directly affects the feasibility of the mission, though it is the least influential factor in this specific value system. While financial constraints exist, the primary objective of this mission is to demonstrate the feasibility of building infrastructure at a large scale. The mission is not designed to minimize spending at the expense of performance; rather, it focuses on establishing a viable method for construction. An initial investment of higher value is considered acceptable if it ensures the payload works effectively and is scalable.

### 2.2.6 Mission Performance Ranking

The following table describes the value system established for the C3 Lunar mission. The opinions of each team member were taken into account, and a value system matrix was generated to prioritize design decisions.

Table 1: Weighted Ranking of Evaluation Criteria.

Criterion	Weight	Rank
Scalability	0.444	1
Impact	0.292	2
Time	0.129	3
Risk	0.081	4
Cost	0.052	5

As can be seen, it was decided that **Scalability** was the most important criterion. This is due to the weight constraints imposed, meaning the payload would have to demonstrate how it could build an infrastructure instead of building it completely. So, scalability has to be important; otherwise, the payload would not be beneficial. The hope is that the payload could be replicated or scaled up to create the complete infrastructure.

**Impact** was ranked second in importance. The impact of a mission ensures that the purpose and significance of the mission are worth the amount of money and effort being put into it. If a mission is of low impact, it is not only harder to get support from potential stakeholders, but it also doesn't advance an end goal in any meaningful way.

**Time** was chosen as the third most important criterion. Time is important due to funding and planning. Depending on the planned time for a mission, it could be difficult to achieve funding. For example, if a mission plans to use water gathered from the moon, but is reliant on the equipment to do so already being there, it limits the timeline of the mission. It is also important to mention that if a mission is planning to take upwards of ten years, but is achieving a small goal, it reduces the chance of funding.

**Risk** was chosen as the fourth criterion due to this mission not involving a crew. This mission was created assuming no people will be near the lander or payload, which greatly reduces the risk. There is still some risk in the lander getting off course and potentially crashing into a satellite or orbital debris and causing damage, but that is low. There is also a risk in the equipment not operating correctly once it reaches its landing site, but that is always a risk in any mission.

The final criterion chosen was **Cost**. This mission is to demonstrate the feasibility of building an infrastructure at a large scale and to demonstrate value. It was not created to try to minimize spending. It focuses on having a viable method for building infrastructure instead of a lower-cost mission that may not work or be scalable.

## 3 Mission Overview

### 3.1 Objectives

The main objectives of this mission are to design a payload for the Griffin lunar lander to help build the infrastructure needed for a permanent lunar outpost. The mission serves as a technology demonstration for In-Situ Resource Utilization (ISRU), specifically proving the feasibility of autonomously manufacturing structural tiles from lunar regolith. These objectives are formulated to address the critical hazard of plume ejecta by creating consolidated landing zones, thereby supporting the sustainability of future Artemis operations.

#### 3.1.1 Key Requirements

The system requirements were derived from the physical constraints of the Griffin Lander payload envelope and the operational necessities of the lunar surface environment. Each of these requirements defines the capabilities that the subsystem must fulfill, serving as the baseline for the mass, power, and autonomy trade studies. The table below lists each of the system requirements for this mission. The first eight requirements represent the necessary objectives that the system must be able to achieve.

Table 2: System Requirements: Displays the Requirements of the System.

System Requirements	
SYS1.0	The system shall have a total mass of under 200 kg.
SYS2.0	The system shall occupy a volume no greater than 75
SYS3.0	The system shall autonomously manufacture structurally sound tiles using In-Situ Resource Utilization (ISRU).
SYS4.0	The system shall accept and process lunar regolith to use as the primary material for tile production.
SYS5.0	The system shall produce hexagonal tiles that meet defined structural and thermal performance standards.
SYS6.0	The system shall operate autonomously for the duration of the mission, including health monitoring and fault recovery.
SYS7.0	The system shall be capable of surviving and operating within the lunar surface environment (thermal and radiation).
SYS8.0	The system shall perform all operations within the allocated peak power and energy-per-tile budget.
SYS9.0	The system should produce one structurally sound tile autonomously within 2 weeks.
SYS10.0	The system should detect and respond to failures with the Griffin Lander.
SYS11.0	The system should store sufficient regolith to produce a 2-3 tile without additional delivery.

As seen in the list of system requirements, the design is heavily constrained by mass and density (SYS1.0, SYS2.0) and the necessity for high-level autonomy (SYS6.0). The requirement to process abrasive regolith

(SYS4.0) and survive the thermal extremes of the lunar surface (SYS7.0) drives the selection of robust mechanical and thermal subsystems.

### 3.1.2 Key Mission Elements

The request for a lunar infrastructure payload allows for significant flexibility in architecture. Unlike a standard rover mission, this objective requires both a rover for collection and heavy industrial processing, which is handled by the stationary system. The choice of a different design process would dramatically affect the concept of operations in terms of the different stages of the operation.

The rover architecture system defines the division of labor. To satisfy the mass constraint (SYS1.0), the system was divided into two distinct units: a lightweight mobile rover for collection and a stationary heavy-duty factory for processing. This split allows the heavy sintering hardware to remain on the lander, reducing the energy cost of locomotion.

The stationary system focuses on the technique for tile creation. The decision was made to utilize microwave sintering (SYS3.0), as it requires no binder material from Earth, fully satisfying the ISRU requirement. This method directly influences the power subsystem design due to the high energy bursts required for heating.

## 3.2 Concept of Operations (CONOPS)

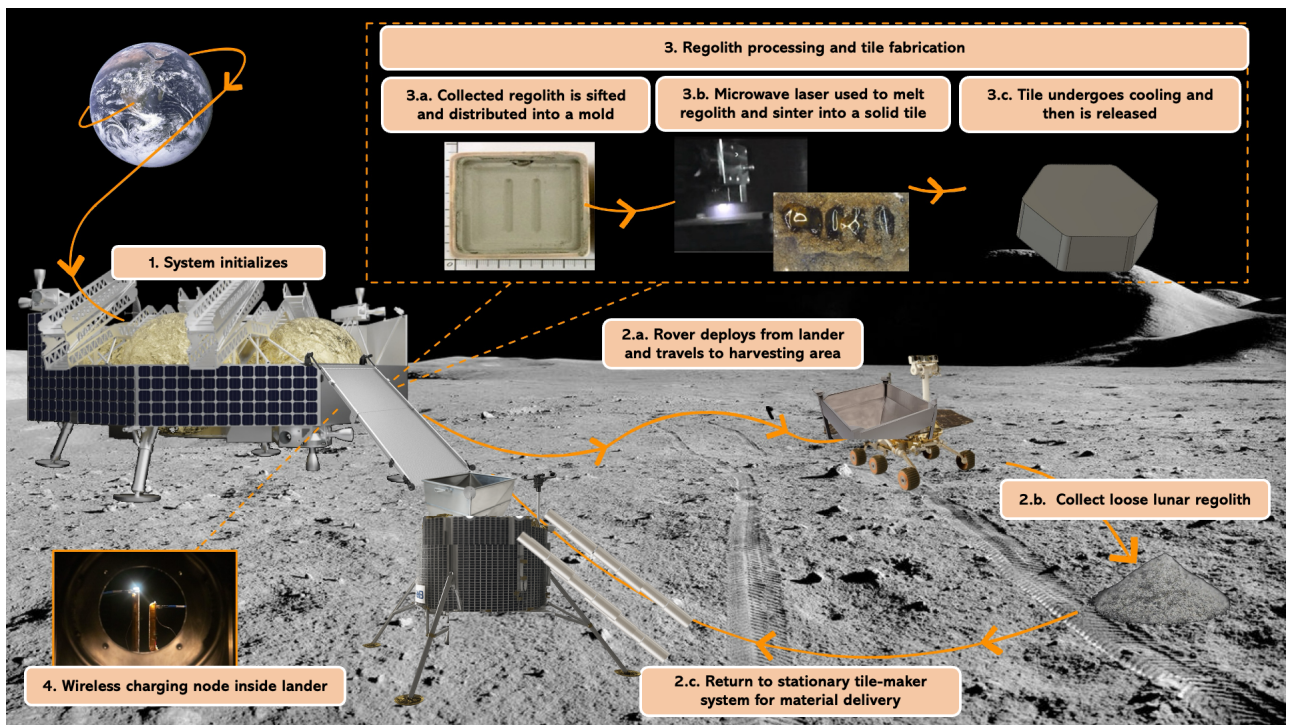


Figure 4: Concept of Operations for the mission.

The mission employs the Griffin Lander to deliver the payload to the lunar surface. Following landing, the system transitions to autonomous surface operations and executes a cyclical operational process designed to collect lunar regolith, process it on-site, and fabricate solid tiles for surface infrastructure applications. An overview of the operational sequence is shown in Figure 4. The concept of operations proceeds as follows:

- 1. Deployment and Initialization:** After landing, the lander performs system health checks and initializes surface operations. Solar arrays deploy to provide power, and the stationary tile-fabrication system is

deployed from the lower deck of the Griffin Lander to the lunar surface.

2. **Regolith Collection:** A small rover deploys from the lander and traverses to a designated harvesting area, where loose lunar regolith is collected using an excavator arm.
3. **Material Transfer and Recharging:** Once loaded, the rover returns to the stationary tile-fabrication unit, docks, and transfers the collected regolith into a hopper via a ramp or elevator mechanism. During docking, the rover connects to a wireless charging node integrated into the lander to recharge its battery.
4. **Regolith Processing:** Inside the fabrication unit, the regolith is sifted using a vibratory screen to remove oversized particles. The processed material is then weighed and distributed into a mold to ensure consistent tile geometry.
5. **Sintering:** A microwave laser system melts and sinters the regolith into a solid tile.
6. **Cooling & Release:** The fabricated tile undergoes controlled cooling to mitigate thermal stresses and prevent cracking. Once cooled, the tile is released onto the lunar surface.

This cycle is repeated throughout the mission, enabling gradual production of surface tiles as the rover alternates between regolith collection and battery recharging. By keeping the primary processing equipment stationary and assigning mobility to the rover, the system maintains operational simplicity while supporting scalable construction of landing pad infrastructure.

### 3.3 Fabrication Trade Study

After deciding on the mission objective of constructing lunar landing pads, VT LUNA needed to select a fabrication method that would allow for the creation of the best landing pads within the power limit and mass budget outlined. The most significant issue is the weight budget of 200 kg. This constraint, given by the RFPs, was the largest driving force in the fabrication selection. After researching the best ways to construct lunar landing pads, it came down to two categories: binders and heating/sintering. After a short research period, binders were ruled out since they require Earth-born materials that typically rely on water or other minerals to mix with regolith. This method would seriously impact the project's scalability, as the mass of these binders would take up a significant portion of the mass budget [10].

With this, VT LUNA decided to look into sintering as the main tile fabrication method. After some quick research, it was found that the two best options were solar and microwave sintering. Solar sintering directly uses optics to focus intense solar light into a beam for heating the regolith until it reaches its melting point, where it then turns into a rigid, glass-like material. Similarly, microwave sintering uses an RF transmitter to send microwaves into the regolith; this heats the regolith and forms structures in the same way. VT LUNA concluded that microwave sintering was the best option to complete the mission objective since it was easier to control the applicator area with a mounted antenna, can work while not in direct sunlight, and uses power systems that would already be needed for the rest of the systems, making it less complex and easier to run with the entire payload [11].

After reviewing these methods, VT LUNA elected to use microwave sintering as the primary fabrication tool. Microwave sintering offers the most control over area, size, shape, and power usage. Its only drawback is power efficiency; however, this is not as much of a concern since there is a surplus of available power. With this, given enough time and constant power, the system can create an effectively unlimited number of tiles, which creates strong scalability and options for future improvements throughout the lifespan of the payload.

Table 3: Fabrication Method Trade Study Summary.

Criterion	Binder-Based Construction	Solar Sintering	Microwave Sintering
Imported Material Mass	High – requires Earth-derived binders	Low – no binders required	Low – no binders required
Compatibility with 200 kg Mass Budget	Poor – consumables occupy a large payload fraction	Moderate – large optical hardware required	Good – RF hardware is mass-efficient
Electrical Power Requirement	Low–Moderate	Low electrical, high thermal	Moderate (~1 kW)
Dependence on Sunlight	None	High – requires direct solar illumination	None
Operational Flexibility	Limited by binder supply	Limited by sun angle and shadowing	High – operates independent of illumination
System Complexity	Moderate – mixing, handling, curing	High – optics, pointing, dust protection	Moderate – RF generation and antenna system
Dust Sensitivity	Low	High – optical surface contamination	Low – sealed RF aperture
Scalability	Poor – limited by binder mass	Moderate – limited by illumination conditions	High – limited by available time and power
Tile Geometry Control	Moderate	Low–Moderate	High – electronically controlled heating
Overall Suitability	Low	Moderate	<b>High (Selected)</b>

## 4 Landing Site Selection

Selecting a landing site will require careful consideration of several factors: sunlight, safety, communications access, thermal conditions, and surface smoothness. The ideal site is one that offers continuous solar illumination, safe and accessible terrain, and proximity to valuable resources such as water ice. Landing pads primarily require stable, flat, and accessible terrain with continuous sunlight for power generation.

For this mission, the landing site must meet the following criteria:

1. Maximum solar illumination
2. Safe and accessible terrain
3. Reliable communication access with Earth
4. Temperature stability for equipment safety
5. Thick, stable, and well-characterized regolith composition

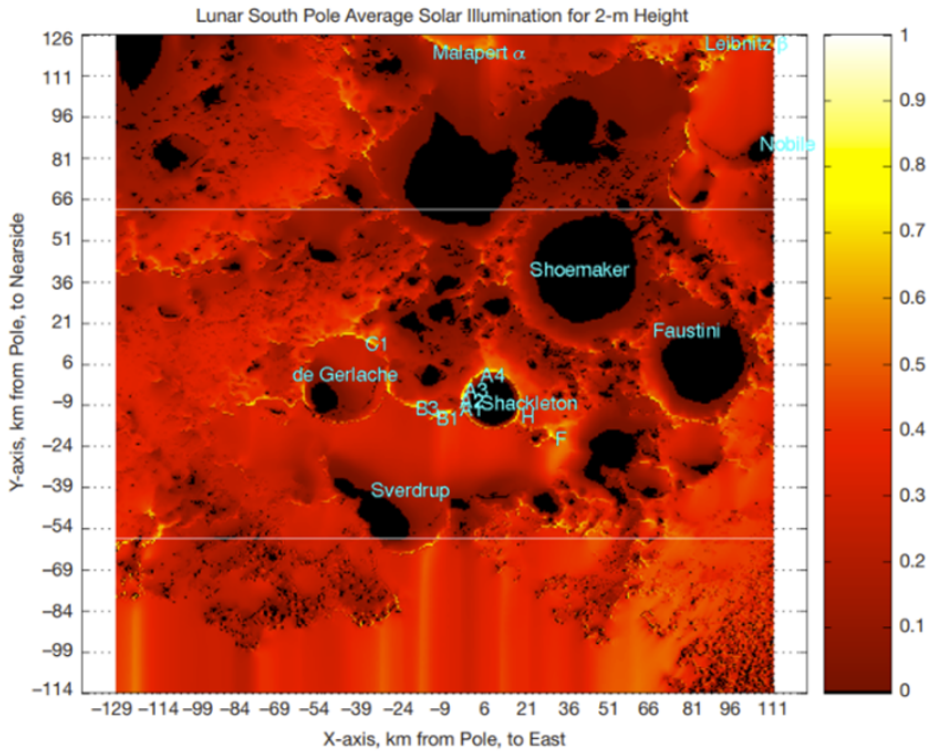


Figure 5: Lunar South pole solar illumination yearly average showing craters with low to no illumination and areas of high illumination on crater rims [12].

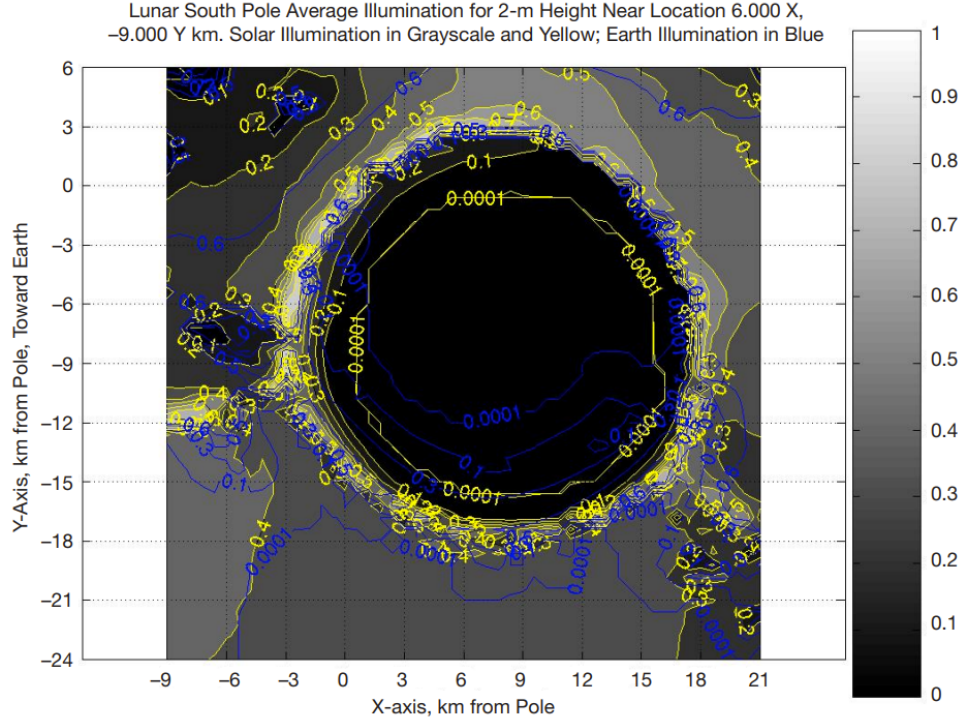


Figure 6: Shackleton crater yearly average illumination further illustrating the differences in illumination throughout a crater at this potential landing site [12].

When choosing where to land and build on the Moon, sunlight remains one of the most important factors. Illumination varies dramatically across the lunar surface, making the poles particularly valuable for solar energy access. Figure 5 shows the average yearly solar illumination for the lunar south pole at a height of 2 m above the surface. The brightest zones, located around the rim of Shackleton Crater and extending toward de Gerlache Crater and the Connecting Ridge, stay illuminated for as much as 85 - 90% of the lunar year [12]. This makes them some of the most favorable locations on the Moon for generating continuous solar power.

According to lunar scientists, the Moon's south pole represents a completely different environment than the equatorial sites visited during the Apollo mission. This new location offers longer illumination, colder shadowed regions, and far greater terrain variability. Sunlight at the Moon's poles is unique, as some areas have near-permanent sunlight, while others experience long periods of darkness. These luminous regions, often called peaks of eternal light, provide nearly continuous exposure to sunlight, making power generation easier and reducing the need for large batteries. They also help maintain more stable temperatures, which is critical for both equipment and human operations.

Figure 6 shows a yearly average illumination map of Shackleton Crater, clearly highlighting that the crater rim receives sunlight more than 80% of the year, while the interior remains in permanent shadow. However, despite its exceptional illumination, landing on Shackleton's rim or adjacent ridges is operationally very risky. The slopes around the crater are steep and uneven, with elevations varying from -3 km to +1.5 km relative to the local mean. So, even small errors in descent trajectory could cause a lander to crash on a slope or in shadowed terrain.

In August 2022, NASA announced thirteen candidate landing regions near the lunar south pole for the Artemis III mission, the first mission to return American astronauts to the lunar surface since Apollo 17 [13]. These initial regions are shown in Figure 7. In October 2024, NASA refined its analysis and narrowed the list to nine potential regions, shown in Figure 8, reflecting more detailed studies of illumination, communications visibility, and terrain accessibility. The nine updated candidates are: Peak Near Cabeus B, Haworth, Malapert

Massif, Mons Mouton Plateau, Mons Mouton, Nobile Rim 1, Nobile Rim 2, De Gerlache Rim 2, and Slater Plain [14].

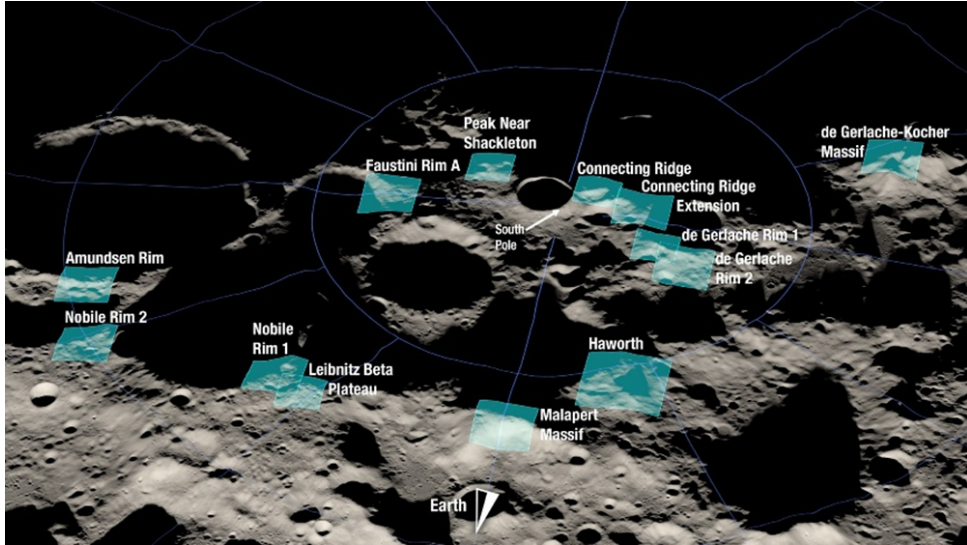


Figure 7: NASA’s 13 candidate landing regions for Artemis III [13].

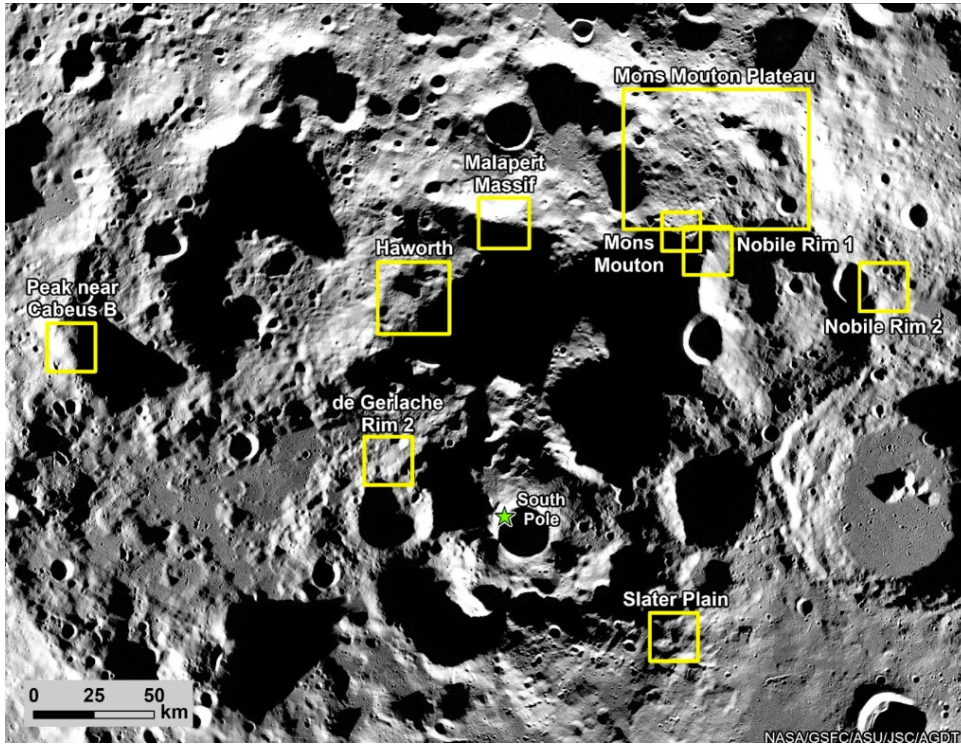


Figure 8: NASA’s redefined candidate landing regions for Artemis III [14].

Although the Peak Near Shackleton site was initially considered one of the most promising options due to its exceptional illumination and strategic location, it has been excluded because of its steep terrain and the operational challenges associated with landing in such areas. Therefore, NASA’s 2024 analysis excluded Peak Near Shackleton from the final list of candidates. Instead, the De Gerlache Rim 2, Mons Mouton Plateau, and Malapert Massif emerged as more practical alternatives, still offering high illumination (70–80% annual

illumination) combined with flatter and more accessible terrain suitable for the construction of early lunar infrastructure such as landing pads.

For this mission, the Mons Mouton Plateau, specifically the Nobile Rim 1 location within the plateau, was selected as the most appropriate site. This region represents the best overall compromise among illumination, terrain safety, communications reliability, thermal stability, and regolith suitability and predictability. Although it receives slightly less sunlight than the Shackleton rim (about 70–80% annual illumination), Mons Mouton Plateau offers far smoother, safer, and more accessible terrain, making it significantly more practical for landing and for constructing landing pads. The site also provides robust line-of-sight communication with Earth, a key requirement for early missions, and sits within operational distance of multiple PSRs in nearby craters such as Haworth, de Gerlache, and Nobile. Additionally, NASA studies indicate that the regolith in this area is thick, stable, and of predictable composition, further supporting its selection for infrastructure development.

De Gerlache Rim 2 and Malapert Massif were not selected because both introduce operational challenges that outweigh their advantages. De Gerlache Rim 2, despite good illumination, has rugged terrain and higher seismic activity, making both landing and construction riskier. Malapert Massif offers excellent Earth visibility but receives less sunlight and is dominated by steep slopes that limit safe landing areas. These factors make both sites less suitable than the broader and more accessible Mons Mouton Plateau.

In short, the best sites for solar power are those near the poles, at higher elevations, where sunlight is almost constant but still accessible and safe for landing. Although the Peak Near Shackleton region remains scientifically valuable due to its illumination and proximity to potential water-ice deposits, its rugged topography makes it unsuitable for initial construction efforts. By contrast, selecting the Mons Mouton Plateau, specifically the Nobile Rim 1 region, provides a balanced and operationally realistic solution for this mission: it maximizes landing safety, supports efficient construction, ensures reliable power and communications, and positions the mission near key resources.

## 4.1 Lunar Regolith

The moon's topography is very complex, with the topological features varying from -8 Km to 10 Km, where the altitude is measured from the elevation of the reference ellipsoid. There are four main geographical maira characters to consider, being Basalt plains, Volcanic origin, High Ti, and Low Ti mare basalts. As the lunar topography varies, so does the chemical composition of the lunar regolith.

Table 4: Lunar Regolith Compound Concentration [15].

Chemical Compound	Concentration (%)
Silicon Dioxide ( $\text{SiO}_2$ )	42–48
Titanium Dioxide ( $\text{TiO}_2$ )	1–7
Aluminum Oxide ( $\text{Al}_2\text{O}_3$ )	12–27
Iron Oxide ( $\text{FeO}$ )	4–18
Magnesium Oxide ( $\text{MgO}$ )	4–11
Calcium Oxide ( $\text{CaO}$ )	10–17
Sodium Oxide ( $\text{Na}_2\text{O}$ )	0.4–0.7
Potassium Oxide ( $\text{K}_2\text{O}$ )	0.1–0.6
Manganous Oxide ( $\text{MnO}$ )	0.1–0.2
Chromium Oxide ( $\text{Cr}_2\text{O}_3$ )	0.2–0.4

#### 4.1.1 Lunar Topography

The different mares can be found by their respective altitudes and can be easily distinguished using a topological map. Topological maps color-code the altitudes and distinctly show different terrain features.

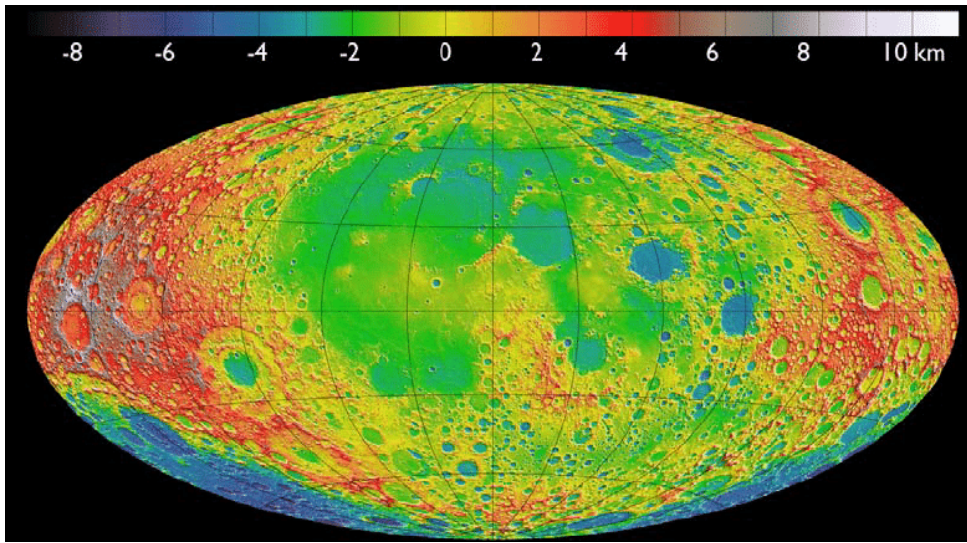


Figure 9: Topographical map of the Moon detailing average altitude deviation [16].

The areas of interest are Highland, Basalts plains, High Ti mare, and Low Ti mares. Basalt plains are seen in Figure 9 in the flat blue areas and are about -6 km in altitude. Highlands are seen in the white side of the spectrum and mostly seen at the south pole and are 10 km in altitude, and the high Ti and low Ti mares range from -4 to -1 km in altitude and are seen in the light blue and green areas.

The basalt plains were formed by impacts that left deep impressions in the lunar mantle, melting it in the process. These impacts created extensive, flat, dark plains like the Tranquillitatis and Serenitatis, and cover roughly 16% of the lunar surface and have a mantle thickness from 30-100 km. These areas are high in Iron Oxide (FeO) and titanium oxide. Because of the thin crust, there is significant surface variation due to exposed magma tubes and flow fronts. Due to the way they are formed, the consistency of the lunar regolith varies widely depending on the impact crater and how far away it is.

High-ti mare is exceptionally high in titanium dioxide and iron oxide. Varying in altitudes from -4 to -1 km. But low in Silicon Dioxide in comparison to Low Ti. High-Ti maria regolith also has excellent properties, being extremely absorbent of microwaves and extremely uniform, sand-like regolith.

Low Ti mare are formed from thick lava sheets and, as a result, are extremely flat without any large terrain features. They are one of the more stable areas of the moon and are low in titanium content. Low Ti mare is most comparable to Hawaiian basalt, with large stable rocks and large granular size, and less abundant loose regolith.

#### 4.1.2 Regolith Chemical Makeup

Table 5: Lunar Regolith Compound Concentrations by Mare[15].

Chemical Compound	Highland	High-Ti Mare	Low-Ti Mare
Silicon Dioxide ( $\text{SiO}_2$ )	44.9	41.0	45.1
Titanium Dioxide ( $\text{TiO}_2$ )	0.5	8.5	2.9
Aluminum Oxide ( $\text{Al}_2\text{O}_3$ )	25.1	12.4	13.1
Iron(II) Oxide ( $\text{FeO}$ )	6.2	16.6	17.0
Magnesium Oxide ( $\text{MgO}$ )	7.5	8.9	9.9
Calcium Oxide ( $\text{CaO}$ )	14.9	11.4	11.7
Other	0.9	1.2	0.3

The chemical makeup of the regolith will affect the melting point. Because the majority of the regolith is metal oxides, they absorb energy very well, having high dielectric loss, and will lose heat much faster than other materials like silica or aluminum. Because the exact mixture depends on the chosen landing location, the exact temperature and method of sintering will be affected [15]. The particle density will also affect how well the sintering process works. Studies using regolith sintering show that an average grain size of  $< 600 \mu\text{m}$  work best with the sintering process. This grain size allows the density to be adequate, so the sintered material will flow into gaps, forming a solid part and improving layer quality. The sintering process melts the regolith, and it forms small drops of molten regolith. If the grain size is too big, there will be gaps between the formed drops, and it will fail at making one cohesive tile.

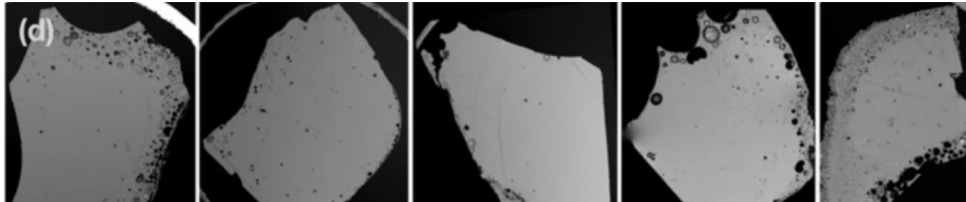


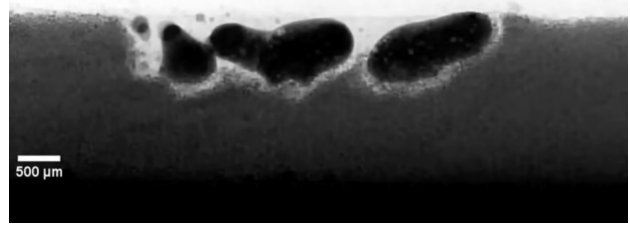
Figure 10: Void holes in sintered products [17].

#### 4.1.3 Regolith Sintering

Heat shrinkage is an issue with lunar regolith [15]. When sintering the regolith, there will be mass loss and volume shrinkage. The shrinkage varies due to the material makeup, time under heat, boiling points, and sublimation temperatures. During sintering, boiling points are essential because if the regolith is sintered at too high a temperature, the tile would become porous due to off-gassing, weakening the tile. That is why it is important to keep the total temperature under the sublimation temperature. Sintering at  $1200^\circ\text{C}$  will lead to 10.1% of the mass being lost, and having the total volume at 1150 for over 96 hours, 50% of the mass will be lost [15]. In addition, overheating the regolith will break down the chemical composition of the regolith [18]. When sintering above  $1000^\circ\text{C}$ , pyrolysis and thermal decomposition of silicate compounds can occur. These processes release gases that form pores seen in Figure 10 within the material, creating voids that weaken the final structure. To mitigate this, a multi-step temperature profile is best, tempering the material and allowing for the pores to fill themselves in [18].



(a) Particle sintering shrinkage.



(b) Particles bubbling and not connecting.

Figure 11: Visual representation of problems with sintering particles such as shrinkage and bubbling [19].

Because of the chemical makeup of the regolith, the base will be silicon dioxide. Silicon dioxide is not very reactive to microwave sintering, so the other compounds are important to increase the efficiency of the sintering process and absorb the heat to speed up the heating. Of the chemical compounds, Iron Oxide and Titanium Dioxide are the most important because they are the most reactive to microwaves.

The lower the percentages of other contaminants, the more homogeneous a tile will be. The chosen landing sight has the highest percentage of Titanium Dioxide and a high Iron oxide concentration. Boiling points are important because if they were to be sintered at too high a temperature, the tile would become porous due to off-gassing, and weaken the tile. That is why it is important to keep the total temperature under the sublimation temperature. Sintering at 1200 °C will lead to 10.1% of the mass being lost, and having the total volume at 1150 °C for over 96 hours, 50% of the mass will be lost.

Figure 11 shows the challenges of the sintering process. When the regolith is heated up, the overall volume will decrease due to the increase in density between the regolith in particle form and in a liquid form. To mitigate the effect of this, the sinter process will make it layer by layer. This will allow for empty volume from shrinkage to be filled in and any gaps from an uneven layer seen in Figure 11 to be filled in. To further mitigate any issues with a porous tile preventing the bubbling issue from forming voids in the completed tile. The bubbling is due to the surface tension of the liquid regolith, which causes the regolith to attract to each other.

Table 6: Boiling Points and Vacuum Sublimation Temperatures of Lunar-Relevant Oxides [20].

Chemical Compound	Boiling Point @ 1 atm (K)	Vacuum Sublimation Temp (K)
Silicon Dioxide ( $\text{SiO}_2$ )	3223	2073
Titanium Dioxide ( $\text{TiO}_2$ )	3245	2173
Aluminum Oxide ( $\text{Al}_2\text{O}_3$ )	3250	2073
Iron Oxide ( $\text{FeO}$ )	3273	1900
Magnesium Oxide ( $\text{MgO}$ )	3873	2173
Calcium Oxide ( $\text{CaO}$ )	3123	1723
Sodium Oxide ( $\text{Na}_2\text{O}$ )	2223	973
Potassium Oxide ( $\text{K}_2\text{O}$ )	1273	572
Manganous Oxide ( $\text{MnO}$ )	3073	1773
Chromium(III) Oxide ( $\text{Cr}_2\text{O}_3$ )	4273	2273

Lunar regolith, being mostly silicon dioxide, provides a great opportunity for future lunar infrastructure. Silicon dioxide has high compressive strength and is inert to most chemicals. It is very stable under thermal

loads with low thermal expansion. Silicon dioxide can be found in uses like concrete, silica reinforcement fibers, and sandstone. Concrete is also used to make landing and launch pad structures and is perfect for the use case of landing pad tiles. The issue with lunar regolith is that other contaminants will weaken the tile, so the smaller the other contaminants' percentages, the stronger and more homogeneous the tile.

Because of the chemical makeup of the regolith, the base will be silicon dioxide [15]. Silicon Dioxide is not very reactive to direct sintering methods or any magnetic fields, so the other compounds are important to increase the efficiency of the sintering process and absorb the heat to speed up the heating. Of the chemical compounds, Iron Oxide and Titanium Dioxide are the most important because they are the most reactive to different forms of sintering methods. The chosen landing sight has the highest percentage of Titanium Dioxide and a high Iron oxide concentration. This is great for methods of sintering, like microwave sintering, because it allows for a greater absorption of the energy that is put into it. The high Iron content helps with polarization for the dielectric response, making the regolith in a sintered state more attracted to each other, helping with creating a uniform layer height [21].

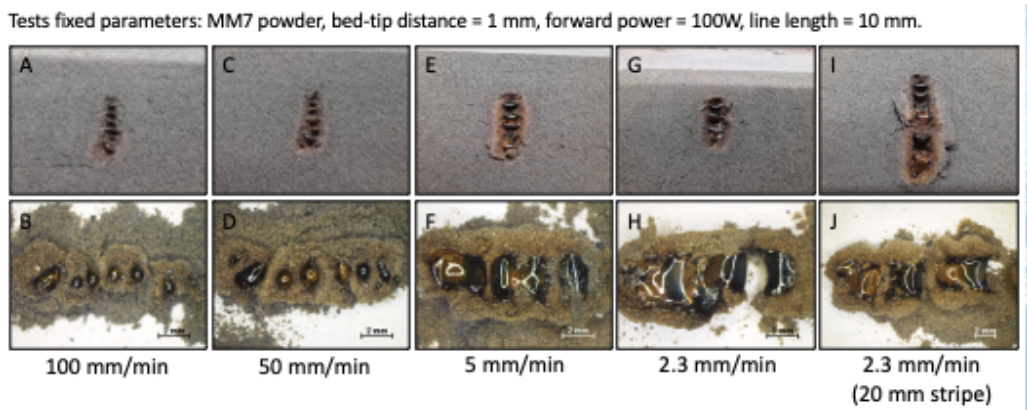


Figure 12: Sintering speed of lunar regolith simulant under microwave heating [22].

Figure 12 shows the sweeping speeds used in a microwave sintering experiment performed by the European Space Agency (ESA) [23]. At 1 kW of power, lunar regolith will be sintered, and the bubbling issue can be solved. It also shows the need to sinter in layers and the shrinking due to the disruption around the sintered material.

The selected landing site, Noble 1, provides the best lunar regolith for the sintering case, lying in the High Ti mare zone. It provides the highest concentrations of both Iron oxide and Titanium Dioxide to increase the effectiveness of the sintering process and lower the levels of other contaminants in the tile. The Iron will allow for an increase in dielectric response of the regolith and allow for the liquid sintered regolith to react with the magnetic field and attract to each other [21]. The High Ti mare has the best loose regolith to collect, leading to an excess to sort and generate an average grain size of  $< 600 \mu\text{m}$ . With a bulk density that would allow for a sintered product without any air voids to weaken the tile. To best sinter the tile, a temperature profile is designed to temper the regolith to allow for gas to escape.

## 5 System Synthesis

### 5.1 Regolith Tile Properties

The requirements for the regolith tiles are derived from two main constraints: the material properties to withstand the applied loads that occur during a launch or takeoff from a targeted 50,000 kg Human Landing System (HLS); and the manufacturing constraints of the stationary tile maker. Therefore, to meet the goals of the project, the following requirements were created.

Table 7: Regolith Tile Requirements: This table displays the requirements of the regolith tiles.

Regolith Tile Requirements (RTR)	
RTR 1.0	The tile must survive the landing of a 50,000 kg Human Landing System (HLS).
RTR 1.1	The tiles shall be able to withstand a sustained vertical pressure of 35.4 kPa from the HLS landing plume.
RTR 1.2	The tiles shall withstand 423.99 kPa impact of HLS landing.
RTR 1.3	The tiles shall withstand 17786.3 kW/m <sup>2</sup> heating from the plume of HLS landing.
RTR 1.4	The tiles shall withstand 25.78 kPa static pressure of HLS after landing.
RTR 2.0	The tiles shall be able to be manufactured utilizing the stationary tile maker and the microwave sintering process with no post-processing.
RTR 2.1	The tiles shall be vertically homogeneous.
RTR 2.2	The tiles shall not have internal angles.
RTR 2.3	The tiles shall be a geometry that tessellates.

A 50,000 kg HLS vehicle was chosen, as this is the vehicle class with the most thorough existing research done on its landing impact effects on a lunar landing pad. However, further research into larger HLS vehicles such as the approximately 100,000 kg SpaceX Starship, which has been selected for the Artemis program, should be conducted once these companies have finalized designs and released technical specifications for their systems [24].

#### 5.1.1 Material Properties

To determine the necessary strength of the tiles, previous research was assessed in which a Finite Element Analysis (FEA) study simulating a landing of a 50,000 kg HLS was conducted [25]. The results of this analysis are listed in the table below.

Table 8: Loading Conditions Experienced by Landing Pad During a Simulated Landing [25].

Timestamp (s)	Max Plume Vertical Pressure (kPa)	Max Plume Heat Flux (kW/m <sup>2</sup> )	Leg Stress (kPa)
0	0.00	0.00	0.00
1	8.85	4,446.58	0.00
2	17.70	8,893.15	0.00
3	26.55	13,339.73	0.00
4	35.40	17,786.30	0.00
5 (impact)	0.00	0.00	423.99 (one leg)
6 (static)	0.00	0.00	25.78 (four legs)

From this data, it was determined that the material requirements of the tile (RTR 1.1-1.4). However, research into the strength of sintered tiles shows results that vary widely depending on the types of regolith used and the exact process used to sinter the regolith. Therefore, to fulfill these requirements, it was necessary to isolate and examine the properties that affect tile strength and determine the optimal characteristics for the tile fabrication process. The primary properties that affect the strength of the tiles are:

# Porosity

The porosity of the tile has been shown to have an extreme effect on the compressive strength of the tiles. An increase in porosity by 10% can cut the compressive strength and failure load in half. [26] A major cause of porosity in the tiles is the particle size of the regolith used to make the tile. When sifted to a particle size below 212  $\mu\text{m}$  the average porosity of the sintered result should be  $\approx 1.44\%$ .

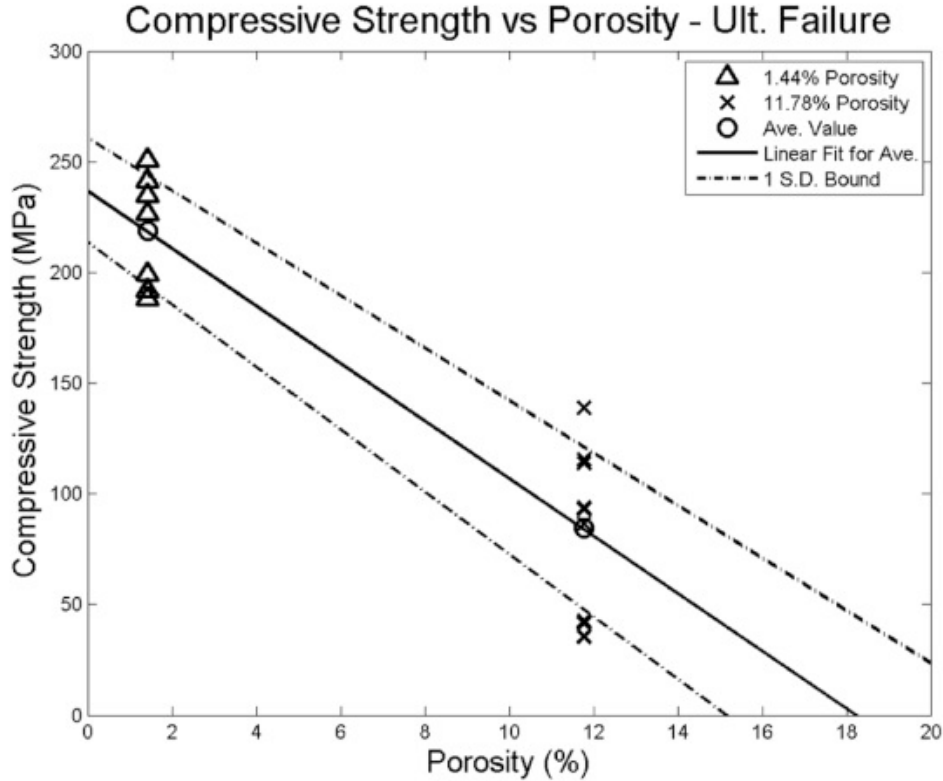


Figure 13: A graph detailing the relationship between compressive strength and porosity [26].

## Sintering Temperature and Regolith Composition

Table 9: Material Properties of Sintered Lunar Regolith Simulant Samples by Temperature [27].

1000°C Radial Shrinkage Percentage	0.84%
1000°C Height Shrinkage Percentage	1.16%
1100°C Radial Shrinkage Percentage	1.85%
1100°C Height Shrinkage Percentage	3.15%
1200°C Radial Shrinkage Percentage	6.17%
1200°C Height Shrinkage Percentage	18.13%
1200°C Compression Modulus (MPa)	55.73
1200°C Compressive Strength (MPa)	21.73

Sintering at a temperature higher than the melting point of most or all of the components of the regolith results in a higher compressive strength for the tile. [28] The melting point for these components tends to be below 1200 °C. [29]. Therefore, for this project, the tiles will be sintered at 1200 °C. Sintering at this temperature can allow molten components to fill voids in the tile, slightly increasing density and decreasing porosity.

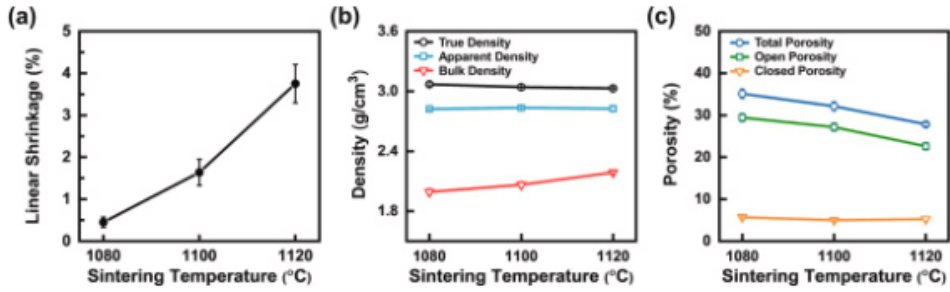


Figure 14: Graphs with relationships between sintering temperature density, shrinkage, and porosity [28].

However, this does create unique challenges in tile design as this high temperature has a side effect of significantly more material shrinkage as seen in the above table [27]. Due to some components of the regolith evaporating and the molten regolith becoming denser and filling the voids between the particles, the volume of the regolith reduces rather significantly. Sintering regolith from highland or mare regolith can give vastly different results. When sintering highlands regolith, the temperature has to be 50 to 100 °C to achieve the same results as when sintering mare.

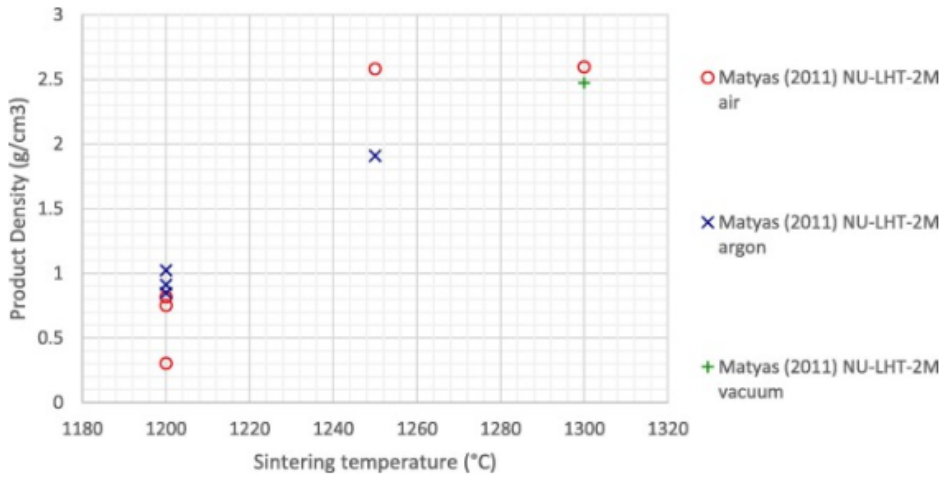


Figure 15: A graph detailing the relationship between highland sintering temperature and density [29].

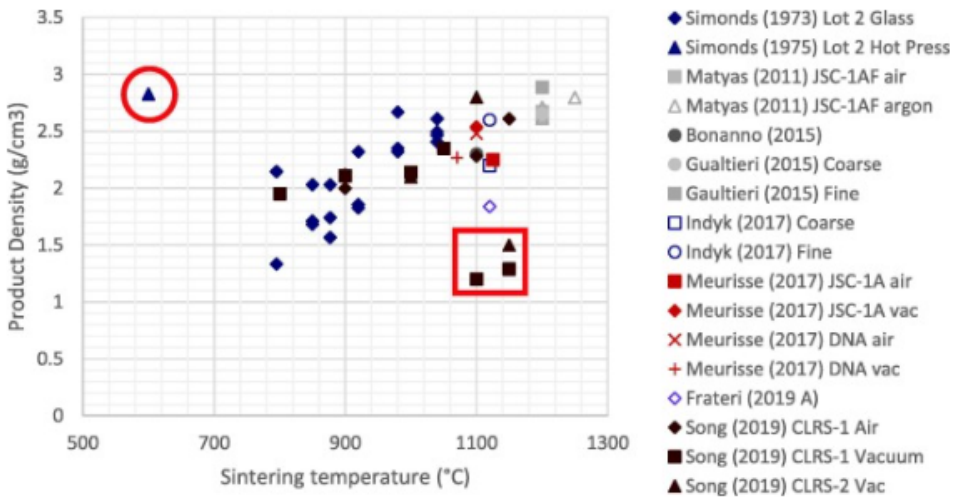


Figure 16: A graph detailing the relationship between mare sintering temperature and density [29].

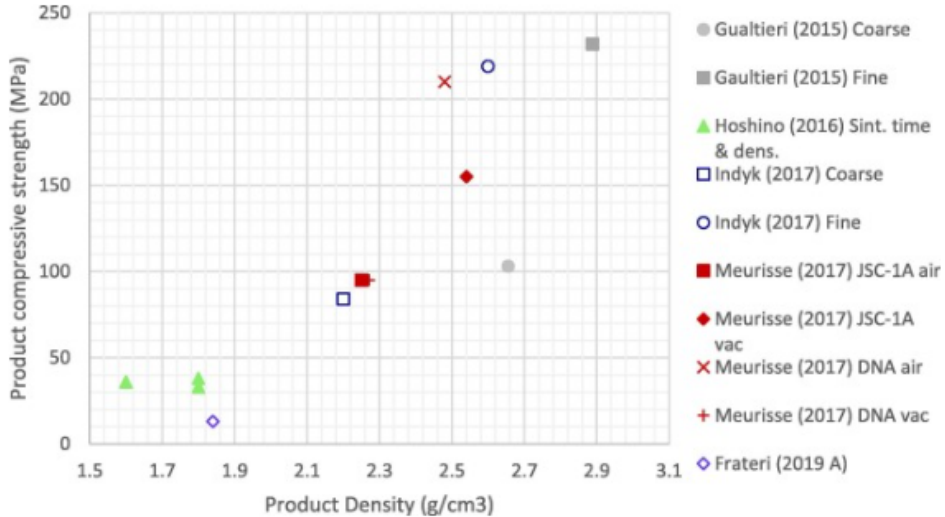


Figure 17: A graph detailing the relationship between regolith density and compressive strength [29].

The compressive strength of regolith when sintered at 1200 °C can vary [27] greatly when considering the environment that the regolith will be collected from; thus, when determining how to satisfy the minimum requirements for the tiles, the minimum possible properties of the tiles should be considered. Throughout all the experiments covered by research conducted by VT LUNA, the low end of the compressive strength of the tiles is about 20 MPa. The bending strength tends to be about 28% of the compressive strength[30], so it will be 5.67 MPa. At this compressive strength, the tile will easily withstand the expected compression forces at any reasonable thickness; thus, the tile's thickness should be determined based on its ability to withstand bending stress due to imperfections in the ground supporting it.

### 5.1.2 Design Properties

The design constraints of the tile design are largely determined by the tile manufacturing process, which imposes unique constraints due to the characteristics of microwave sintering and of the specific tile maker's design, resulting in RTR 2.0. As the design is building tiles through compressing layers and subsequently sintering small splotched areas to form layers, vertical homogeneity is therefore necessary, as any non-uniform designs in the mold would cause difficulty in this compression and microwave sintering process, resulting in RTR 2.1. The aforementioned radial shrinkage of the tiles by approximately 6.17% during the cooling process imposes additional constraints on tile design [27]. As the tiles will shrink inwards horizontally, any internal angles of the mold would therefore be put under pressure by these shrinking tiles, which would result in damage to either the mold or the tile. Therefore, the tiles shall not have internal angles resulting in RTR 2.2.

As there is only one tile maker with a singular mold, only one tile design will be able to be produced. Therefore, the tile produced should be capable of independently forming a solid surface, so the tile shall be a geometry that tessellates, resulting in RTR 2.3.

### Our Tile Design

Based upon these requirements, the tile design is a normal hexagon with a circumscribed radius of 0.15 m, a depth of 0.106 m, and a 25 mm fillet applied to the hexagonal corners as depicted below.

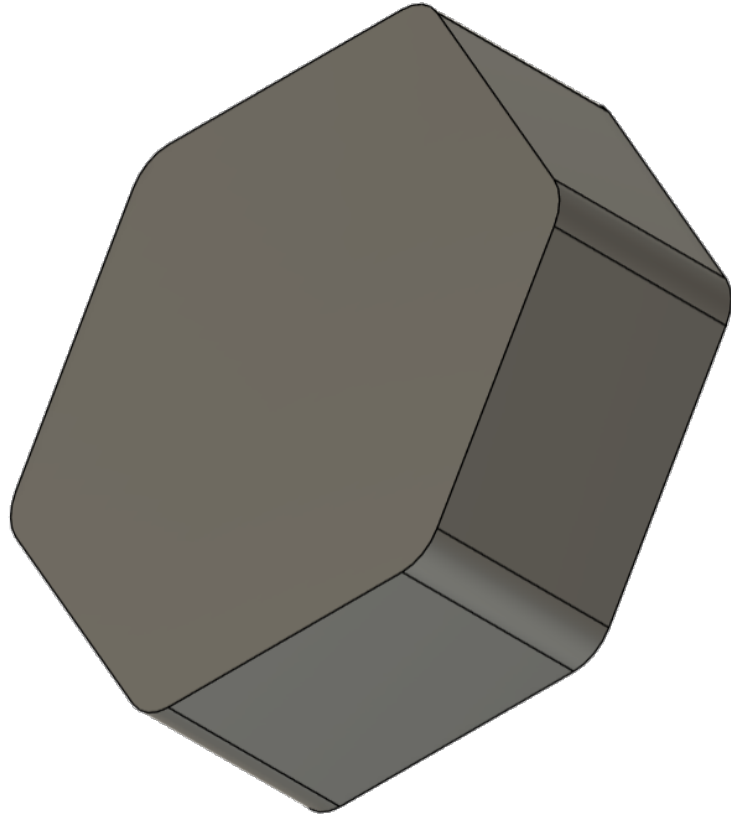


Figure 18: Image of the tile design, a normal hexagon with a circumscribed radius of 0.15 m, a depth of 0.106 m, and a 25 mm fillet.

This design fulfills RTR 1.0 as it can withstand the 423.99 kPa impact outlined in RTR 1.2 as calculated in equation  $t = \sqrt{\frac{K p_{max} \pi r^2}{\sigma_{bending}}} * safety factor$  [31] with K being .398 and the safety factor being 2.3 which is the maximum expected load and therefore fulfills RTR 1.1 and RTR 1.4 as well as they are lesser loading conditions. This design also fulfills RTR 1.3 as it's surface area is approximately the same as the tiles used in a research paper where thermal analysis was conducted showing that sintered regolith tiles are capable of withstanding intense heating as expected from a rocket plume where "the maximum surface temperature ( 700 K) is confined within a central circular area of about 0.5 m in diameter" [32]. This design also fulfills RTR 2.0 as it does not vary vertically, satisfying RTR 2.1; does not have any internal angles, so it satisfies RTR 2.2; and it is based upon a normal hexagon, which is a shape that tessellates, so it satisfies RTR 2.3.

Aspects of the design that the design was unable to accurately quantify for this report include the lateral forces and stresses the tile will undergo, and the thermal expansion characteristics that will occur during landings. Furthermore, "acoustic waves are known to propagate within rocket plumes. However, no publications currently provide data on these waves in the lunar environment," which is another unknown factor that could disrupt tiles [25]. To mitigate these unknowns, the design incorporated fillets that reduce stress concentrations, and by using a hexagon rather than a square or triangle, which also tessellate but have more acute angles, these stress concentrations are further reduced, which will help mitigate the risk of failure from both thermal expansion and lateral forces imposing stress on the tiles.

## 5.2 Sintering Model

### 5.2.1 Justification

Understanding the required power of all the subsystems is an integral part of ensuring the feasibility of this mission and its architecture. The most power-intensive and complex subsystem is the microwave sinterer. The sinterer must be able to heat 8,268 cm<sup>3</sup> of regolith to 1,200 °C. The power required to heat the entire tile simultaneously would exceed the Griffin lander's power output, rendering it impossible. To enable the creation of a tile, sintering will be done in thin layers. Within each layer, about a fifth of it will be sintered at once. With this approach, the instantaneous power draw is low enough to allow the power to be sourced exclusively from the Griffin lander.

Table 10: Required Nomenclature for the Model Equations.[33][34][35][36]

Variable	Symbol	Unit	Type	Dependencies	Value
Power Density	$P$	$\frac{W}{m^3}$	Found	$K, f, E, k', \tan(\delta)$	N/A
Power Draw	$P_s$	W	Found	$P, \eta, V$	1000
Energy Required	$J$	kWh	Found	$P_s, t$	36.9
Heating Rate	$\Delta T$	°C/s	Found	$P, \rho, CP$	N/A
Heating Time	$t$	s	Found	$T_0, T_t, \Delta T$	132734.5
Instant Temperature	$T$	°C	Found	$T_0, \Delta T$	N/A
Initial Temperature	$T_0$	°C	Defined	N/A	0
Target Temperature	$T_t$	°C	Defined	N/A	1200
Dielectric Constant	$k'$	N/A	Material Property	$T, f$	N/A
Loss Tangent	$\tan(\delta)$	N/A	Material Property	$T, f$	N/A
Density	$\rho$	$\frac{kg}{m^3}$	Material Property	$T$	3000
Specific Heat Capacity	$CP$	$\frac{J}{kg \cdot K}$	Material Property	$T$	700
Tile Area	$A_t$	$m^2$	Tile Property	N/A	0.078
Layer Thickness	$h_L$	m	Tile Property	N/A	0.001
Layer Count	$n_L$	N/A	Tile Property	$h$	106
Tile Thickness	$h$	m	Tile Property	$h_L, n_L$	0.106
Spot Count	$n_s$	N/A	Tile Property	$A$	5.45
Tile Volume	$V$	$m^3$	Tile Property	$A, h$	0.008268
Applicator Area	$A_a$	$m^2$	Hardware Property	N/A	0.0143
Microwave Frequency	$f$	Hz	Hardware Property	N/A	$915 \times 10^6$
Electric Field Strength	$E$	$\frac{V}{m}$	Hardware Property	$A_a, P_s$	22404.96
System Efficiency	$\eta$	N/A	Hardware Property	N/A	0.25
Free Space Permittivity	$\epsilon_0$	$\frac{F}{m}$	Constant	N/A	$8.854 \times 10^{-12}$
Equation Constant	$K$	$\frac{F}{m}$	Constant	$\epsilon_0$	N/A

Table 11: Core Modeling Equations Required to Relate the Sintering Process to Lunar Regolith Material Properties.[34][33]

Eq.	Expression
(1)	$P = KfE^2k'\tan(\delta)$
(2)	$\Delta T = \frac{P}{\rho CP}$
(3)	$P_s = \frac{PV}{\eta}$
(4)	$t = \frac{T_t - T_0}{\Delta T}$
(5)	$J = P_s \cdot t$
(6)	$K = K' - jK'' = K_\infty + \frac{K_0 - K_\infty}{1 + (j\omega\tau)^{1-\alpha}}$

### 5.2.2 Method

To model the power required and the time required to sinter a single tile, several key inputs must be defined, including the tile geometry, microwave hardware properties, and regolith material properties. The power absorbed by the regolith is given by Equation (1), and the heating rate is given by Equation (2)[34]. These two equations form the foundation of the model, as they directly relate the hardware properties of the microwave system to the material properties of the regolith. Using these equations, the model can be expanded to determine the instantaneous power draw, the time required to sinter a layer or full tile, and the total energy required, using equations (3),(4), and (5), respectively.

The modeling process becomes more complex when the temperature dependence of regolith material properties is considered. While most variables in the core equations are either constant or can be controlled, several regolith properties depend on temperature, including density, specific heat capacity, dielectric constant, and loss tangent. For the purposes of this model, the temperature dependence of density and specific heat capacity is considered negligible, as these properties change by relatively small amounts over the temperature range of interest. In contrast, the dielectric constant and loss tangent are strongly temperature dependent, and accurately modeling these relationships is critical to producing a useful model[34].

The temperature dependence of the dielectric constant and loss tangent is specific to lunar regolith and must be obtained from experimental data. A NASA study conducted in 1973 measured these properties as functions of temperature and frequency using Apollo lunar samples[33]. This study provides the functional form used to describe these relationships, specifically the Cole-Cole frequency distribution model, shown as equation (6), but does not provide closed-form equations[33]. Instead, the relationships are presented graphically. To obtain usable multi-variable functions, data points were extracted from these figures using the free online tool WebPlotDigitizer and exported as .csv files[37]. These data were then processed using a custom MATLAB script to perform curve fitting and obtain a total of sixteen coefficients: eight for the dielectric constant function and eight for the loss tangent function. Comparison of the fitted functions to the extracted data showed a relative accuracy of approximately 90%.

All remaining material properties, as well as the microwave operating frequency, were obtained from experimental literature and treated as constant values in the model/[35][36]. Any uncertainties in the model were intentionally treated conservatively to ensure that predicted power, energy, and time requirements were not underestimated. The electric field strength was treated as a function of the microwave applicator area, defined

as the area being sintered simultaneously, and this value was optimized later in the modeling process.

Once a constant value or temperature-dependent function was defined for each variable, the rate of temperature change became a function of temperature alone, resulting in a differential equation. To numerically solve this relationship while allowing temperature-dependent properties to influence the heating rate, a time-stepping loop was implemented in the MATLAB script. The model calculates the temperature increase and power consumed at each one-second interval and updates the current temperature and cumulative energy until the target temperature is reached. Because the available experimental dielectric data only extends to 500 °C, a linear interpolation approach was used beyond this temperature, treating the final values obtained from the numerical loop as constants[33]. The initial iteration of the model produced estimates for peak power draw, total energy required, and total sintering time.

A second iteration of the code was then created to optimize the total time to sinter one tile. This was done by treating power draw as a known value and implementing the relationship between applicator area and electric field strength. This allowed for the creation of a vector spanning all possible values for the applicator area, running the model for each one, and then plotting the Applicator areas against the total time taken. Due to the electric field strength being dependent on the applicator area, it is recalculated for every applicator area value. This provides both an estimate for the time it takes to create a tile and the optimal hardware to meet those requirements. After debugging the logic and adding a heat dissipation model to ensure the instantaneous heating remains high enough to reach the target temperature, the following results were obtained.

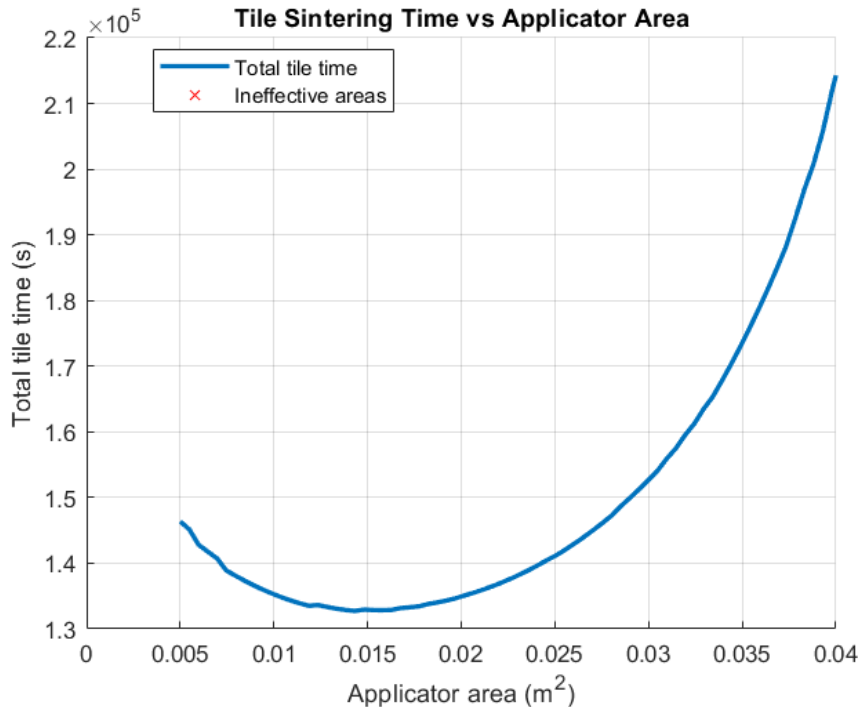


Figure 19: Model figure graphing the total time to sinter one tile against the Applicator area that resulted in that time, the trough shows the optimal applicator area

### 5.2.3 Results

For a hexagonal tile with a face area of 0.078 m<sup>2</sup>, a depth of 0.106 m, and a layer depth of .001 m. The optimal applicator area was 0.0143 m<sup>2</sup> as shown in Figure 19, resulting in an electric field strength of 21,012.20 V/m. The optimal applicator area results in 5.45 sinter cycles per layer, each taking approximately 3.8 minutes. When extrapolated across the 5.45 cycles per layer and 106 layers, the total time to create one tile is 36.9 hours.

These estimates are controlling for power draw at 1kW, which is about 20% of the available system power. The relationship between power draw and time elapsed is linearly inversely proportional, meaning that if 4kW were to be allotted to the microwave, the time estimate would shrink to about 9.2 hours per tile. Importantly, these estimates provide both a reasonable timeline for the sintering process and useful hardware requirements. Given that the sintering is the least proven aspect of the system architecture, these estimations suggest not only that the system is possible, but it is also well within the weight, energy, and time constraints of this mission. The model also helps to illustrate the scalability of the design, with access to power grids or multiple systems drastically reducing the timeline of the construction process.

### 5.3 General Architecture Trade Study

In order to complete the mission objective outlined and use ISRU to create lunar landing tiles, several general architectures were considered during the design process. In this section of the report, VT LUNA will outline these different design options as well as their strengths and weaknesses, and give a justification for the final design before diving into the details of the chosen design. These architectures will fall into the following categories: Independent Rover, Umbilical Cord, Dock to Charge, and Stationary.

#### 5.3.1 Independent Rover

In the independent rover architecture, the construction rover carries its own primary power system and operates autonomously within the local mission area. Power is typically provided by body-mounted or deployable solar arrays coupled with onboard energy storage (batteries and/or capacitors). The rover is responsible for executing the full construction task cycle—regolith collection, transportation, tile fabrication support, and placement—without requiring a physical tether to the lander during normal operation.

This architecture closely mirrors many historical planetary rover missions, such as the Opportunity and Perseverance. This heritage is important as many technological hurdles are well understood and have been overcome in previous missions, giving the design a layer of security. The rover is designed as a self-contained asset: in addition to power, it carries its own computing, communication, mobility, and construction tooling. Mission operations are typically constrained by the rover’s daily energy budget, local illumination conditions, and thermal environment.

Table 12: Strengths and Weaknesses of the Independent Rover Architecture.

Pros	Cons
<ul style="list-style-type: none"> <li>• High Mobility and Range: Limited solely by solar capabilities and energy margins, can access a variety of regolith sources and multiple pad sites</li> </ul>	<ul style="list-style-type: none"> <li>• Mass and Complexity: Must carry solar arrays, and large batteries, increasing mass, volume, and potential failure points</li> </ul>
<ul style="list-style-type: none"> <li>• Heritage: Architecture aligns with many conventional Mars and lunar rover missions(solar and batteries), and design benefits from existing patterns.</li> </ul>	<ul style="list-style-type: none"> <li>• Energy Limited Operations: Construction activities and mobility are bound by the rover’s own power generation and storage. High-power processes required, such as sintering, excavating, and conditioning, may require long charging periods or may not be possible at all.</li> </ul>
<ul style="list-style-type: none"> <li>• Scalability: Multiple rovers can be added to work in parallel operations</li> </ul>	

Ultimately, the mass and, more pressing, power concerns drove VT LUNA away from this design. It had its merits, no doubt, but this architecture was far more suited for the exploration and science missions it was initially designed for, not for energy-intensive construction processes. The idea of on-board solar panels seemed

redundant when the Griffin Lander had its own power generation capabilities, far greater than deployable panels could provide. Finding a way to harness that was essential for the completion of the mission objective. This is not, however, the end of the independent rover concept, as it will make an appearance in the final design of VT LUNA.

### 5.3.2 Umbilical Cord

In the Umbilical Cord architecture, the rover remains physically tethered to the lander via a power cable during operation. The solar array on the lander hosts the primary power generation system, and the rover draws continuous power through the umbilical. The operation is similar to a high-power tool on a long extension cord. A spool mechanism may manage the tether, or it may be laid on the lunar surface.

This architecture is well-suited to tasks that occur in a relatively compact work zone near the lander. Since power is provided continuously, the rover can support energy-intensive tools and processes without needing to stop for a recharge.

Table 13: Strengths and Weaknesses of the Umbilical Cord Architecture.

Pros	Cons
<ul style="list-style-type: none"> <li>• High Continuous Available Power:</li> </ul> <p>Has access to a large, lander-based power array, enabling sustained operation of high-power tools (i.e., sintering unit, conditioning equipment, excavation implements)</p>	<ul style="list-style-type: none"> <li>• Limited Mobility:</li> </ul> <p>Operational radius is constrained by tether length. Complex terrain and other obstacles may further reduce the operational area.</p>
<ul style="list-style-type: none"> <li>• Simplified Rover Power System:</li> </ul> <p>The tether almost eliminates the need for an on-board battery, significantly reducing its weight.</p>	<ul style="list-style-type: none"> <li>• Tether Management:</li> </ul> <p>Cable is exposed to abrasion by regolith, mechanical damage from rocks or wheels, and potential entanglement with rover chassis, lander legs, or other obstacles. Damage to the tether results in mission failure</p>
	<ul style="list-style-type: none"> <li>• Interference With Other Assets:</li> </ul> <p>The tether concept drastically decreases scalability and can interfere with future lunar operations, as additional rovers, landers, or human crews will have to navigate around a web of cables.</p>

The umbilical cord design provides a much-needed solution to the problem of rover power draw. However, the added complexity from the tether system provides a logistical hurdle that VT LUNA deemed too difficult to overcome.

### 5.3.3 Dock to Charge

The Dock-to-Charge architecture removes the need for deployable solar panels by making the primary power plant the lander itself, and makes the rover act as a 'sortie' vehicle. The rover now carries a medium-sized battery capable of performing short trips and discrete construction tasks before returning to the lander to dock and charge.

In this concept, operations are structured as sortie cycles. The rover departs from the lander fully charged, travels to the work site, executes a defined construction sequence (i.e., gather regolith, tile placement, sintering),

and then returns to the lander to recharge.

While docked, the rover can take advantage of higher continuous power from the lander's solar array for higher power draw tasks such as sintering.

Table 14: Strengths and Weaknesses of the Dock to Charge Rover Architecture.

Pros	Cons
<ul style="list-style-type: none"> <li>• Access to High Power:</li> </ul> <p>Access to a large solar array from lander, energy-intensive activities can be carried out when the battery is fully charged</p>	<ul style="list-style-type: none"> <li>• Limited Range:</li> </ul> <p>Effective operational radius is constrained by the need to maintain energy reserves to return to the lander, limiting construction capabilities to short, sortie-style construction.</p>
<ul style="list-style-type: none"> <li>• No Tether:</li> </ul> <p>No risk of a power tether being dragged over terrain, reduces all risks associated with tether from umbilical cord concept</p>	<ul style="list-style-type: none"> <li>• Charging Downtime:</li> </ul> <p>While the rover is docked and charging, it is not performing any construction tasks</p>
<ul style="list-style-type: none"> <li>• Scalability:</li> </ul> <p>Many rovers of this design can be used in parallel to complete construction objectives while others are charging, increasing productivity and reducing downtime</p>	<ul style="list-style-type: none"> <li>• Docking Complexity:</li> </ul> <p>Requires a robust mechanical and electrical interface between the rover and the lander. Needs alignment tolerances, dust-tolerant connectors, and guidance features, all adding a layer of complexity</p>

#### 5.3.4 Stationary Tile Maker

In the stationary tile maker architecture, the "rover" is no longer a rover and becomes a fixed manufacturing plant attached to the lander. It possesses no mobility capabilities and is instead optimized for regolith conditioning and tile fabrication. Power and data are provided through a short harness from the lander's primary power system.

Removes navigational capabilities and mechanical degrees of freedom, and focuses solely on producing structurally sound tiles with high power availability

Table 15: Strengths and Weaknesses of the Stationary Tile Maker Architecture.

Pros	Cons
<ul style="list-style-type: none"> <li>• Simplified Mechanical Design:</li> </ul> <p>Eliminating mobility capabilities allows the design to focus on the manufacturing process</p>	<ul style="list-style-type: none"> <li>• Limited Access to Regolith:</li> </ul> <p>A stationary system cannot relocate to new regolith sources and is reliant on excavating from its nearby vicinity via arm or auger. If regolith near landing site is not usable, mission objectives are compromised.</p>
<ul style="list-style-type: none"> <li>• High Power and Duty Cycle:</li> </ul> <p>Hardwired to lander's large solar array, enabling near-continuous operation and high tile throughput without energy limitations of mobile platforms</p>	<ul style="list-style-type: none"> <li>• Local Congestion Around Lander:</li> </ul> <p>Concentrating manufacturing activities near the lander can lead to a cluttered environment</p>
<ul style="list-style-type: none"> <li>• Scalability:</li> </ul> <p>This system can easily be scaled up with multiple stationary tile makers working in parallel without inhibiting one another</p>	

This design greatly simplifies the completion of mission objectives by focusing on tile fabrication and benefits greatly from continuous access to high-power. However, without any mobility capabilities, serious concerns arise.

### 5.3.5 Final Choice

VT LUNA settled on a hybrid architecture, pulling elements from each design that worked well and discarding aspects that were not useful. This hybrid retained most of its general architecture from the stationary tile maker concept and will thus be referred as such. VT LUNA deemed that the most essential aspect of the challenge in order to complete mission objectives was ensuring the feasibility of continued tile fabrication. However, the drawbacks of this design were duly noted, and several key adjustments were made to compensate for the shortcomings of the stationary tile maker's original design. Namely is the addition of a small rover with a small on-board battery and dock to charge capabilities. This small rover's primary objective is to gather regolith from optimal sites and then return and deposit said regolith into the stationary tile maker. Upon completion of its regolith deposit, if needed the rover will then navigate back to its dock and charge.

## 5.4 Regolith Collection System (Rover)

The collection system relies on a small autonomous rover designed to retrieve regolith and transport it to the stationary processing plant. The rover operates in a continuous loop, and there will be four major steps to this process.

The first step is the deployment; the rover will leave the dock/Griffin lander in search of regolith. The navigation system will be initialized as soon as the rover deploys to guide the rover to the best location to retrieve the regolith. The navigation system chosen consists of Wheel Odometry and IMU, which will be used for obstacle detection and alignment. The rover will only be traveling short distances, between the collection site and the lander, which is why this navigation system was chosen. It is lightweight and provides sufficient accuracy while consuming low amounts of power compared to other navigation methods. The tires of the rover were also chosen with the location in mind. Rigid aluminum wheels with grousers are the tires chosen, because the landing site will have loose lunar soil. This type of tires will ensure traction and allow the rover to travel between operational locations.

The second step is collecting the regolith. Once the rover reaches the excavation area, it will begin the collection process. This will be done via a three-joint robotic arm, consisting of a shoulder pitch joint, elbow pitch joint, and wrist tilt joint. These joints will supply 15–30+ Newton-metre, 8–10 Newton-metre, and 2–3 Newton-metre of torque, respectively, which will allow the arm to scoop loose regolith and transfer it to the hopper. The hopper will be constructed of aluminum alloy, similar to the three-joint robotic arm. The hopper will be designed to hold 16 kilograms of regolith, but the rover will return to the stationary tile maker when there are 14.5 kilograms of regolith stored. This accounts for regolith spillage in the rough terrain. The arm will have to have multiple scoops per trip, because the scoop can only hold up to 3 kilograms of regolith at a time.

The third step in the rover cycle is the return to the stationary tile maker. The path will be short and repeatable, which will allow the rover's navigation to be as accurate as possible. Once the rover reaches the stationary tile maker, it will align itself with a telescoping ramp. The ramp will be designed to guide the rover in the exact position needed to dump the regolith into the stationary tile maker's hopper.

Once the rover is aligned to the ramp, it will travel up to the stationary tile maker's hopper. It will start the dumping procedure, starting with the actuation of the hopper's tilt motor. The hoppers will invert, causing the collected regolith to be released in the reception hopper. After the regolith is received, the material-processing sequence starts, which includes screening, weighing, and ultimately microwave sintering inside the stationary tile maker. While this sequence is taking place, the rover will remove itself from the ramp to begin the next step of the cycle.

The last step is dependent on the stationary tile maker; it will communicate to the rover to tell it the next

step needed. The rover will either go into dock-to-charge mode, where it will interface with a charging node integrated into the lander, and the 24 V lithium-ion battery will have the energy consumed during the previous cycle replenished, or it will be told to continue gathering regolith. The stationary tile maker can hold enough regolith to create multiple tiles, so depending on the rover's charge level, it could be beneficial to continue to gather regolith. If the station does tell the rover to charge, it will travel to the charging node and not only charge but run basic diagnostic checks. Once the charging is complete, the rover will resume autonomous operations. It's also important to note in the lunar night, the rover will return to the charging node, not to charge, but to enter night mode. This will prevent the damage that could be done to the rover over cold nights.

#### 5.4.1 Excavator Arm Design

The rover's excavation arm is a three-joint mechanism designed to scoop loose lunar regolith and transfer it into the hopper. Its three joints consist of a shoulder pitch, elbow pitch, and wrist tilt joint, each driven by its own brushed DC motor coupled to a planetary gearbox. This system will provide the needed torque for digging and dumping while keeping the system simple and lightweight.

The arm was designed to be long enough to reach the surface in front of the rover, scoop regolith, and clear the hopper rim during dumping, while still folding compactly on the lander deck. The arm was modeled as three main segments: the shoulder joint to the elbow joint, the elbow joint to the wrist joint, and the wrist and scoop segment. It was decided that the main material used would be aluminum alloy, the same as the on-board hopper. Below is a table showing the length of each section and its estimated weight.

Table 16: Rover Arm Segment Properties and Torque Influence.

Segment	Length (m)	Mass (kg)
Upper Arm (Shoulder → Elbow)	0.40	1.2
Forearm (Elbow → Wrist)	0.35	0.9
Wrist + Scoop Assembly	0.20	0.6
Regolith Payload	—	3

The arm is being designed to carry regolith, so the maximum regolith that can be carried was taken into account in the payload. The effective payload at the wrist was taken as 3 kilograms in torque calculations. Each worst-case loading scenario for the arm joints was taken into account in the torque calculation, to ensure the motor chosen for each joint would be successful in all possible case scenarios.

The torque requirements at each joint were estimated by treating the arm as a set of point masses located at the centers of each segment and at the scoop. Static torque was found for each. A safety factor of 3 was applied to the static torque estimate to account for other factors. Some of these potential factors are soil resistance when cutting into regolith, Dynamic loads when starting/stopping motion, and Friction in joints and gearboxes. Below is a table showing the results of the torque calculation for each joint.

Table 17: Torque Requirements and Motor/Gearbox Selection for Rover Arm Joints.

Joint	Cont. Torque (Nm)	Peak Torque (Nm)	Motor + Gearbox Class	Sources
Shoulder (Pitch)	15–20	30+	24 V brushed DC gearmotor with 80:1–100:1 planetary gearbox	[38], [39], [40]
Elbow (Pitch)	8–10	15–18	24 V brushed DC gearmotor with 50:1–70:1 planetary gearbox	[38], [41], [42]
Wrist (Tilt)	2–3	4–5	12–24 V brushed DC gearmotor with 20:1–30:1 planetary gearbox	[43], [44]

As can be seen in the above table, each joint will use a different motor and planetary gearbox, because each has different mechanical roles. The shoulder joint (pitch) is the main lift joint that will raise and lower the arm with a regolith-filled scoop. The elbow joint (pitch) is the middle joint; it will extend and retract the forearm section during scooping and when positioning over the hopper. The final joint, wrist joint (tilt), will control scoop orientation for cutting into the soil and for controlled dumping into the hopper.

For each joint, a DC Motor and a planetary gearbox were chosen over other options due to the high torque density this system applies, and it is very lightweight[38]. Systems like this are also known for being comparably simple and reliable, making them the perfect choice for this mission[38].

#### 5.4.2 Tires and Mobility System

Multiple tires were considered for the rover, each having different advantages and disadvantages. The primary options were rigid aluminum wheels (with grousers), flexible mesh/spring wheels, rubber, and elastomer-Based Inflatable or solid Tires. Rigid aluminum wheels with grousers were selected as the best design for this mission. The decision was based on mass, durability, thermal performance, maneuverability, and previous missions in similar environments to this mission[45, 46, 47].

For the design, the wheels would be roughly 0.8 kilograms per wheel, with a 0.27 m diameter and 0.08 m width. This tire type stood out from others due to its performance in loose granular lunar soil and its zero failure modes related to pressure, puncture, or outgassing[47]. While these were important factors in the final decision, these wheels were chosen because they require minimal thermal attention and are structurally simple enough to withstand repeated loading cycles[46].

Flexible mesh/spring wheels are a woven stainless-steel mesh supported by an internal spring structure. They inflate structurally by elasticity rather than air pressure. While these tires have many pros, such as being very lightweight and having a large history of successful use, they were not chosen. This is due to the tight mass envelope and the repeated regolith-transfer cycles[46]. While this wheel is great for crewed mobility, this mission needed a more rigid and durable wheel.

Rubber/elastomer-based tires are terrestrial-style solid rubber tires, honeycomb tires, or inflatable tires. They have good shock absorption and have high traction on rough terrain, but were also not chosen for this mission. This is because they can not survive lunar vacuum or thermal conditions the rover would undergo[47]. They are also not suitable for long-term missions [47].

Overall, rigid aluminum wheels are the correct choice because they have maximum durability, predictable traction, thermal immunity, low system complexity, and a history of successful missions[45, 46]. The rover will be traveling short distances, carrying heavy payloads, and needs reliable tires. Rigid aluminum wheels are the perfect balance between performance, robustness, and mass constraints.

#### 5.4.3 Navigation System

The rover navigation system was designed to provide reliable and low-power navigation for repeated trips between the excavation site and the stationary tile maker. The rover will be going over short, predictable distances repeatedly, meaning the navigation system had to prioritize simplicity, robustness, and low computational overhead instead of high-precision mapping or long-range mobility. The navigation system has two major components: Wheel Odometry and an Inertial Measurement Unit (IMU).

Wheel Odometry measures how far each wheel has rotated and converts this rotation into an estimate of distance traveled and change in heading [48] [49]. This is very important because it gives an estimate of the position and speed of the rover while it is traveling. It also has low computational cost and no complex sensors, which is ideal for a rover like this one [50] [38]. It is important to mention that Odometry accumulates error (“drift”) over time due to wheel slip, uneven terrain, and encoder noise[51] [49]. This will not be an issue in

this mission because of the small distance that will be traveled. IMU is a compact sensor package that has accelerometers and gyroscopes that measure linear acceleration and angular velocity[49]. It will be used to stabilize the rover's estimate of heading, help maintain scoop orientation, and provide an independent reference to compensate for Odometry drift[52]. Part of the reason it was chosen is that IMU works regardless of lighting, dust, and environmental obstruction[53].

A potential component that may be added to the design next semester is the camera and LiDAR package, which in this case would be a fixed forward-facing optical camera and a small LiDAR unit mounted on the rover. The camera would provide image data while the LiDAR would return distance measurements to nearby obstacles[51] [54]. This component's main jobs would be to provide obstacle detection during travel and to make precise distance and alignment information when approaching the stationary tile maker. Camera and LiDAR packages have been used for exploration, but in this case, they would be used exclusively for local situational awareness and docking[55]. This is still being researched to see if it is needed for the rover, because while it would be helpful in navigation, it may not be needed, and it would add more mass.

LiDAR and Visual-LiDAR Odometry was also considered as an option for the rover's navigation[52]. This approach would involve using LiDAR point clouds to build 3D maps of the environment while tracking the rover's location[54] [56]. It has been used in many advanced planetary rovers and robotic exploration systems before, so it is well tested [48] [56]. While it is much more robust to wheel slip than other methods and can provide full 3D terrain awareness, it was ultimately decided that this system wouldn't work for this mission. This LiDAR requires heavier hardware compared to other methods and has higher power, processing, and memory requirements[52].

In summary, the navigation system selected for this mission provides an excellent balance between capability, reliability, and mass efficiency. Many more advanced methods were evaluated, like LiDAR, but their mass and power requirements made them unsuitable for this rover. The combination of Wheel Odometry and IMU fills all of the navigation needs while remaining low mass and low power, making it the perfect navigation system for this mission[49] [53].

#### 5.4.4 Hopper and Storage

The rover's regolith storage unit will be a hopper, capable of holding approximately 16 kg of regolith per trip. It's essential to note that while the hopper is capable of carrying 16 kg of regolith, it will only carry 14.5 kg of regolith per cycle. This accounts for spillage due to the rough terrain. The amount of regolith stored per trip was decided because 13 kilograms of regolith is needed to make one panel. 14.5 kilograms will give room for regolith getting lost in the transfer process, and the stationary tile maker still receives enough regolith to make a panel every trip. The hopper will be 35 by 25 by 12 centimeters with walls 2.0 millimeters thick and floors 2.5 millimeters thick. This is thick enough to prevent holes from forming in the hopper due to wear, and small enough not to have a large impact on the mass budget. The hoppers' projected mass is 1.36 kilograms, which is ideal for this rover.

The hopper also has several requirements: it must withstand repeated impacts from regolith loading, survive extreme lunar temperature swings, and remain lightweight enough to fit within the rover's mass limits. This means material selection was very important. The mechanical properties, manufacturability, thermal behavior, and mass efficiency of several materials were compared to find the best option.

Aluminum alloy was evaluated first because it has an excellent strength-to-weight ratio and has been used in aerospace structures[57]. It has a density of  $2.66\text{--}2.8 \text{ g/cm}^3$ , which allows the hopper to remain lightweight [58]. Aluminum is also known to perform well in lunar thermal environments [59], and is highly machinable. It has been tested with Lunar dust stimulants, and while there was wear shown, that is to be expected in most materials[60].

Stainless steel was also considered because of its strength and toughness. Because of the steel's strength, it would easily withstand regolith impacts and the bending loads generated during dumping operations[61]. Stainless steel also has good thermal resilience, which is important considering the thermal conditions on the moon. However, its density is 7.8–8.0 grams per centimeter cubed, which is almost three times the previously stated aluminum density[62]. If stainless steel were used, the hopper would be unacceptably heavy, which could take several kilograms away from other rover subsystems. The additional weight would also increase the load on actuators, tilt motor, and chassis, causing the torque and power requirements to be higher than needed. For these reasons, stainless steel is not a reliable material for the hopper.

Titanium alloys were also considered because of their strength-to-weight ratio and corrosion resistance[62]. Titanium alloys have a density of 4.4–4.5 grams per centimeter cubed, which is heavier than aluminum but lighter than stainless steel. But due to Titanium's thermal conductivity being roughly one-tenth that of aluminum, this material was taken out of consideration. Thermal conductivity is important because the temperature changes can create steep temperature gradients across the hopper in titanium alloys[63, 64].

Composite Materials were the final material considered because they have extremely low mass and high stiffness. But, composites have new challenges under lunar environmental conditions, so it was decided that this idea was not viable. Polymers are brittle at extremely low temperatures, and the thermal cycling that they would face on the moon can lead to micro-cracking or delamination[60]. Composites also have poor abrasion resistance compared to metals, which would pose a problem with regolith particles[65].

After considering aluminum, stainless steel, titanium alloys, and composite materials, it was decided that aluminum alloy was the best choice for the rover's hopper. It is a great balance between low mass, structural durability, manufacturability, and thermal resilience[57]. While the other options had their strengths, the mass constraints and thermal conditions make them not a viable choice for this mission.

#### 5.4.5 Power System

The rover must operate independently of the Griffin lander and the stationary tile maker for extended periods of time, meaning it must store enough power for actuation, navigation, and communication. So the power system was designed to prioritize reliability, long cycle life, and compatibility with the stationary charging infrastructure integrated into the Griffin lander.

Before the dock-to-charging method of charging was chosen, many methods were considered. The solar panel was a potential method, but it was discounted due to its mass and mechanical complexity. While it would provide the needed energy, the Griffin lander has solar panels that the rover can use, making it redundant. An extension cord method was also considered, but due to the rover traveling around the stationary tile maker, it was discounted. There would be a risk that the rover could get stuck on its own cord or wrap around the tile maker. The Rover utilizes a dock-to-charge system built into the Griffin lander, which reduces the rover's mass.

The rover will be powered by a 24 V, 20 Ah lithium-ion deep-cycle battery pack, providing approximately 480 watts-hours of usable energy[66] . This amount of energy will allow the rover to perform cycles before requiring a recharge while still maintaining reserve power for heaters, communications, and navigation sensors. Lithium-ion was selected because it has a high energy density and has been used in previous missions[66]. The battery has a mass of 3.6–4.9 kilograms, which fits well into the mass budget[66].

The voltage of the battery needed was found by finding the peak power usage of each component and summing them together. It's important to mention that it is unlikely every component will be consuming peak energy at the same time. For example, while the rover is traveling to the excavation site, the arm won't be in use, and when the arm is in use, the motor used for driving won't be in use. Meaning many components will not be consuming energy at the same time.

As it can be seen in the above table, the total peak power the rover will consume is 339 W. The 24 V, 20 Ah

Table 18: Rover Subsystem Peak Power Consumption.

Subsystem / Component	Peak Power (W)	Sources
Main Autonomy Computer (Jetson Orin Nano 8GB)	15 W	[67, 68]
Drive Motor Controller MCU	1 W	[69]
Arm & Hopper Controller MCU	1 W	[70]
Safety / Power MCU	0.5 W	[71]
Radio / Communications Module (XBee-PRO 900HP)	1 W	[72]
Sensor Suite (IMU + cameras + depth/LiDAR optional)	10 W	[73, 74]
Drive Motors (4 DC gearmotors)	160 W	[40]
Arm Motors	100 W	[75]
Hopper Tip Motor	50 W	[76]
<b>TOTAL Peak Power</b>	<b>339 W</b>	—

lithium-ion deep-cycle battery pack provides approximately 480 watt-hours of usable energy, which is well over 339 watts [66]. This will give the rover enough power to go through multiple cycles before charging is needed.

#### 5.4.6 Computer systems

Four computers are needed for this rover: the main autonomy computer, the drive motor computer, the arm/hopper controller, and the safety and power supervisory computer. All are needed to make the rover function, but each requires different computing power. The computer requiring the most is the main autonomy computer, because it is responsible for high-level decision-making, navigation, perception, and coordination of subsystem activities

Table 19: Rover Computing Subsystems, Responsibilities, and Mass Estimates.

Subsystem / Computer	Hardware Type	Key Sensors / Actuators Connected	Mass	Sources
Main Autonomy Computer	Jetson Orin Nano (8GB)	<ul style="list-style-type: none"> <li>Cameras (RGB/Depth)</li> <li>LiDAR / Stereo</li> <li>IMU</li> <li>Odometry from Drive MCU</li> </ul>	0.15–0.25 kg	[77]
Drive Motor Controller (MCU)	Microcontroller (STM32 / Teensy class)	<ul style="list-style-type: none"> <li>Wheel motors</li> <li>Wheel encoders</li> </ul>	0.02–0.08 kg	[78, 79, 80, 81]
Arm & Hopper Controller (MCU)	Microcontroller	<ul style="list-style-type: none"> <li>Arm motors</li> <li>Hopper tip motor</li> <li>Joint encoders + limit switches</li> </ul>	0.02–0.08 kg	[71, 79]
Safety / Power Supervisory MCU	Small MCU	<ul style="list-style-type: none"> <li>Battery sensors</li> <li>Power relays / MOSFETs</li> </ul>	0.01–0.04 kg	[71, 82, 83, 84]

The Jetson Orin Nano (8GB) was chosen as the main autonomy computer. It is supported by a network of

microcontroller units (MCUs) that independently manage motor control and safety-critical functions[77]. This will make sure the rover can achieve every step in the cycle without additional help. This device was chosen because it provides plenty of room for future autonomy upgrades like enhanced obstacle detection or improved arm trajectory planning[77].

It was decided that a microcontroller would be the computer for the Drive motor computer, Arm/Hopper controller[78, 79, 80, 81, 71]. This is because these systems are less complex. The hopper will only be expected to tilt; the arm, on the other hand, is more complicated. It is a three-joint arm running autonomously, but this is still a less complex responsibility of the Main autonomy computer. Research into which microcontroller is best for the rover will continue into next semester, but the power and weight requirements can be estimated based on microcontrollers for sale.

A safety and power supervisory computer is needed to monitor battery voltage, temps, and to cut motor power if the main autonomy computer fails[71, 82, 83, 84]. A small microcontroller unit will be the computer for this. The power and weight requirements of the small microcontroller unit were estimated based on small microcontroller units for sale[71, 82, 83, 84]. The selection of which microcontroller is needed will happen next semester.

#### **5.4.7 Structural Frame and Chassis Design**

The structural frame and chassis of the rover will be a major design focus for next semester. The frame will need to support each component and the loads generated during excavation, transport, and dumping operations. The material selection and the geometric layout will be chosen/picked with stiffness, durability, and weight in mind. The chassis will be designed to mitigate dust intrusion, reduce abrasion, and prevent dust accumulation around and on sensitive components. These structures will heavily influence the weight of the rover, so an estimate was incorporated into the mass budget. This is subject to change, but the mass estimate is likely over the needed mass. It was created this way to err on the side of caution. Next semester, a CAD-based structure will be created to make sure the rover is following the mass budget limitations.

#### **5.4.8 Thermal Management and Heating System**

A Thermal Management and heating system will be needed due to the temperature changes on the moon. At the current landing site, lunar night is expected to be 14 days, meaning the rover would have to maintain enough heat to prevent damage to itself. The rover will not be collecting regolith in lunar night; it will go into night mode in the Griffin lander charging port. Night mode will be the rover turning off all electronic components, except the heating systems.

While the heating system needed hasn't been selected, there have been design decisions made with it in mind. The battery was picked, keeping the extra power the heating system will need in mind. The mass budget was also created with the heating system in mind. The heating systems needed are still being researched, taking into consideration what their weight effects would be. A final decision on heating systems is expected to happen early next semester

#### **5.4.9 Summary**

While there is still more work to be done on the rover design, a solid foundation has been established. Each component was evaluated based on its mass, durability, energy efficiency, and lunar environmental constraints in the component selection process. Next semester, work will continue to try to design and model the rover.

## 5.5 Manufacturing System (Stationary Tile Maker)

The Stationary Tile Maker is designed as a material-handling and fabrication system that has the autonomous capability to convert lunar regolith into dense, microwave-sintered paving tiles suitable for landing pad construction. The architecture consists of four major subsystems 1. Collection 2. Conditioning 3. Sintering 4. Cooling. Together, these components create a controlled material pathway that ensures regolith moves from unprocessed, variably graded soil into a uniform, compacted, and sintered tile with consistent mechanical properties.

### 5.5.1 Collection

The first stage system, after the collection rover completes its process, is the collection system. This system is characterized by a telescoping ramp and a reception hopper. At the entry point, the telescoping ramp provides the collection rover with an adjustable and reliable means of ascending to the top of the stationary tile maker for regolith deposition. The design will include chamfered guide rails to ensure stability upon ascent. Given the variability of the lunar terrain, and to reduce reliance on the precision of the rover's navigational systems, the ramp bottom will feature funnel-like self-centering geometry to guide the rover into the tracks and reduce the margin of error. The ramp must remain structurally rigid under the rover's mass while minimizing weight and stored volume. Because of this criterion, an aluminum alloy such as 6061-T6-Aluminum is an advantageous material selection. Additionally, its surface is treated to reduce electrostatic adhesion, given the dielectric charge of lunar regolith.

The reception hopper functions as the first buffering and storage unit in the system. It will receive raw regolith from the rover and then provide a controlled outlet to downstream processes. Its geometric structure will consist of a two-stage inverted pyramid. The internal geometry of the hopper is essential to its design to prevent flow obstruction and inconsistent discharge. The upper stage, or deposit stage, of the hopper will have a wide mouth with an area of  $0.4 \text{ m}^2$  acting to catch any regolith plume that may result from the initial deposit. This will then narrow down to an inner funnel with a mouth area of  $0.15 \text{ m}^2$ , and wall angles of  $70^\circ$  to prevent lunar regolith bridging and to promote mass flow under reduced lunar gravity, as this steep angle is above the angle of repose of lunar regolith by a significant margin[85]. Because bridging and arching tendencies increase in reduced lunar gravity, the hopper relies on a combination of steep interior surfaces, conductive coatings, and a small vibratory motor (coupled to the screener) to maintain flow reliability. The hopper also decouples rover delivery cycles from tile production rate thus maintaining operational continuity and reducing idle time. This is done through a slide gate system that releases when the stationary tile maker has sufficient charge for a sintering cycle and engages when the system is in idle mode, or sufficient regolith for a tile has been processed. This slide gate is attached to a flange which is connected to the first stage of the conditioning subsystem, the vibratory screener.

### 5.5.2 Conditioning

#### Vibratory Sifter

Downstream of the hopper, the vibratory sifter serves as the first stage as well as the primary material-conditioning subsystem. The main purpose of this subsystem is to remove over-sized regolith aggregates and ensures that the regolith that makes it to the sintering stage is below the required particulate size ( $< 600\mu\text{m}$ ) as defined in the materials properties section. Having a uniform particle size is a critical step in the conditioning process. It results in predictable compaction behavior and allows for effective microwave sintering. This is due to the fact that particle size and its distribution strongly influences the powder packing behavior, densification rates, and the resulting microstructure and mechanical properties of sintered materials. Studies show

that controlled particle-size distributions facilitate consistent compaction and more uniform densification during sintering, which is critical for predictable mechanical performance [86][87].

The design also relies on a multiple stage sifter. The first stage will consist of a laser-cut 6061-T6-Aluminum plate with a cut diameter of  $2.0\text{ mm}$ . This laser-cut plate architecture is chosen because it is more durable and abrasion-resistant than a woven mesh of aluminum. This first sifting stage exists to remove large clasts of regolith and oversized rocks from the selection process. The secondary stage will also be made from a laser-cut Aluminum plate, reducing the cut diameter to  $0.8\text{ mm}$ . The second stage is more fine-tuned sifting while still removing larger particles and reducing the maximum load that will be incurred by the more delicate fine mesh woven final stage. The final stage will consist of a woven mesh with a cut diameter of  $550\text{ }\mu\text{m}$ . This diameter is slightly below the required particle diameter of  $600\text{ }\mu\text{m}$ . This design choice is to ensure that no abnormally shaped particles above the required diameter make it through to the final selection and ensure uniformity in the chosen regolith.

It is assumed that the maximum load that the sifter will undergo at any given point is the mass of a single tile, being  $13.3\text{ kg}$ . The deck size chosen is  $0.4\text{ m}$  relatively arbitrarily to match the mouth of the hopper inlet, as well as to ensure that the regolith can be evenly distributed for sifting. The frequency range of  $25 - 50\text{ Hz}$  is typical for many lab applications of finely tuned sieves, which typically operate between  $1,400$  and  $3,000$  cycles/min [88]. The sifter uses a vibratory motor, operating at a frequency  $50\text{ Hz}$ . By operating in the upper end of this range, the motor ensures that the vibratory motion will overcome cohesive forces. Given the geometry of the sifter, the maximum mass load, and the required frequency, the motor specifications can be found. After research into lab-grade sieves with similar specifications as the vibratory sifter being implemented on the stationary tile maker, the following motor specifications were found [89].

Table 20: Vibratory Sifter Motor Specifications.

Type:	DC Brushless Motor
Power Rating:	$125 - 180\text{ W}$
Excitation Frequency:	$50\text{ Hz}$
Amplitude:	$1 - 3\text{ mm}$

These values come from  $0.4\text{ m}$  three-stage lab sieves with a mass rating of  $25\text{ kg}$ . This means that the power rating for the motor is conservative and will have excess power capabilities to operate as the single vibratory motor for the whole system (including reception hopper and weigh bin). The brushless DC motor is optimal for lunar conditions as it has a longer life cycle than a brushed motor, and no contact points for lunar regolith to interfere with. The main adjustment to make a motor of this specification space grade is by introducing a dry lubricant such as Molybdenum Disulfide (MoS<sub>2</sub>).

## Weigh Bin

Once regolith is passed through the sifter, it enters the weigh bin, where precise mass metering will take place. the top flange of the weigh bin will be mated to the vibratory screener and sealed with a slide gate. This slide gate will release, and the weighing bin will accumulate material until the required mass for a single tile is reached ( $13.3\text{ kg}$ ). This is to ensure that each sintering cycle has a consistent volumetric and mass input. Four compression load cells will be mounted to the bottom of the weigh bin to provide mass measurement. This subsystem plays a vital role in tile reproducibility. The bottom of the weigh bin will be equipped with an outlet rotary gate. When the target mass is reached, this rotary gate will dispense  $1/106$  of the total mass, or  $12.55\text{ g}$  at a time. This metric comes from the layered sintering process of  $1\text{ mm}$  layers per sintering cycle for a total tile height of  $106\text{ mm}$ .

## Sinter Mold

The final stage of the conditioning process occurs in the sinter mold itself, where the regolith undergoes the compression stage. The mold consists of a stainless steel plate with a recessed geometry mirroring the tile dimensions. The stainless steel mold is chosen due to its high temperature resistance and microwave reflective capabilities. This is essential for the sintering process, in which as much microwave energy as possible must be directed and absorbed by the regolith. When the regolith is deposited into the mold, another vibratory motor mounted to the mold engages to ensure even distribution of the regolith in the mold. At this point, a motor-driven zirconium ceramic plate applies pressure to the regolith to densify the material and reduce voids. This enhances microwave absorption uniformity and final structural integrity. The ceramic plate is chosen due to the architectural requirement that the compression plate must be mounted below the phase array, but must not impede the microwave process. The transparency and temperature-resistant qualities of zirconium ceramic make it an optimal choice.

### 5.5.3 Microwave Sintering

Our microwave sintering process will use layer by layer sintering to create a solid tile body capable of withstand multiple rocket landings and takeoffs. These tiles will be replaceable and repairable, making the entire system highly scalable. In order to fully utilize this system, the design had to create a complete microwave system capable of producing multiple tiles per lunar day. The setup uses volumetric dielectric heating to evenly heat and sinter the regolith, creating strong bonds both within and between layers.

One of the most important design decisions for the device was selecting an RF generator. To do this, the design needs to verify both the power level and operating frequency required for effective sintering. Using commercially available options as a baseline, the design selected the 1 kW power range, as it is scalable and supported by a wide range of available space-grade and industrial hardware. The selected operating frequency is 915 MHz. This frequency provides improved penetration into lunar regolith and, most importantly, does not interfere with the Griffin Lander's 2.45 GHz WLAN communication system. Similar to the power selection, this frequency band is commonly used and supported by mature hardware. All baseline calculations for the sintering process were therefore performed assuming a 1 kW, 915 MHz RF generator [90].

After selecting the RF generator, an appropriate applicator for delivering microwave energy to the regolith had to be chosen. Initial research focused on waveguide arrays and small localized applicators; however, a key challenge quickly emerged. While a large tile area must be sintered, only a small region can be processed at one time due to power constraints. One potential solution is to use a small applicator that physically moves across the tile surface, sintering localized regions sequentially to build up a full layer. The primary drawback of this approach is the added mechanical complexity and increased number of failure points introduced into the lander system. A single jammed or damaged mechanical component could jeopardize the entire mission.

To address this limitation, alternative solutions within the antenna design space were investigated, leading to the selection of a phased-array antenna approach. Phased-array antennas consist of large panels that use constructive and destructive interference to steer and manipulate electromagnetic waves without mechanical motion. Based on this concept, an array shaped to match the tile geometry can be used to electronically move the microwave applicator across the tile surface during sintering. This approach enables full-layer sintering without any moving parts, while maintaining low power usage and minimizing system complexity. Further analysis showed that additional power margin exists within the system, allowing for the potential use of a higher-power RF generator to significantly reduce tile production time [91, 92].

#### 5.5.4 Cooling Subsystem Architecture

##### Overview and Process Content

Since the microwave produces an enormous amount of thermal energy, it can cause the system to overheat and destroy key components such as the electronics. Following the high-temperature sintering process within the microwave cavity, the newly formed regolith tile must undergo a controlled thermal reduction before it can be safely ejected from the stationary payload assembly. As the final operational stage prior to tile release, the cooling architecture serves two critical functions: ensuring the structural integrity of the manufactured tile by mitigating thermal shock, and protecting the payload's sensitive electronics from residual heat soak. The design must achieve these goals while adhering to the strict mass and power constraints of the lunar environment.

##### Design Trade Study

To select the optimal thermal management strategy, an in depth trade study was conducted evaluating five different cooling architectures.

Table 21: Trade Study Comparison of Potential Cooling Architectures for Regolith Tile Manufacturing [93].

Cooling Method	Description & Key Points	Pros/Cons
Rapid Cooling	Material is cooled quickly after sintering, often by exposure to ambient or forced air.	Fast and energy-saving, but can cause cracking or reduced material strength.
Single-Step Cooling	Material is cooled at a constant rate from sintering temperature to room temperature.	Simple, but may not prevent thermal gradients or internal stress.
Hybrid/Assisted Cooling	Combines direct and indirect cooling (e.g., susceptor-assisted heating, external heat sinks).	Can improve uniformity of tiles, but adds system complexity.
Cold Sintering	Uses low temperatures and pressure with a transient liquid phase for densification.	Energy efficient, but not suitable for all regolith or ceramic compositions.
Multi-Step (Staged) Cooling	Cooling is performed in controlled stages with pauses or slower rates at critical temperature intervals.	Reduces thermal stress and improves quality and uniformity.

- **Rapid Cooling:** The first method evaluated was rapid cooling, utilizing exposure to ambient lunar conditions or forced convection. While this approach offers the fastest cycle times and significant energy savings, analysis indicated it induces severe thermal shock. The rapid contraction of the outer layers relative to the core creates high tensile stresses, leading to the tiles cracking and significantly lowered

mechanical strength in the final tile.

- **Single-Step Cooling:** The single-step cooling profile, where the material is brought down to ambient temperature at a constant, linear rate. Although this simplifies the control logic, it lacks the adaptability required for the complex thermal properties of lunar regolith. A constant rate does not account for the non-linear phase transitions of the material, failing to prevent localized thermal gradients and residual internal stress.
- **Hybrid / Assisted Cooling:** A more advanced option involved hybrid cooling, combining direct radiative methods with indirect conductive heat sinks (susceptors). This method showed promise in improving thermal uniformity across the tile surface. However, the integration of these external heat sinks adds substantial complexity and mass to the stationary payload, conflicting with the lightweight design requirements.
- **Cold Sintering:** Briefly explored cold sintering, a process utilizing low temperatures and high pressures with a transient liquid phase to achieve densification. While highly energy-efficient, this method was deemed unsuitable for the specific mineralogy of lunar regolith and the constraints of the microwave-based heating architecture.

### Selected Architecture: Multi-Staged Cooling Architecture

To address the limitations of individual methods, the VT LUNA payload will utilize a Multi-Staged Cooling Architecture. This hybrid approach integrates the strengths of the evaluated concepts into a phased thermal management strategy tailored to the regolith sintering cycle.

The process initiates with a rapid conductive transfer stage, utilizing a thermal sink interface to quickly bring the tile below critical transition temperatures immediately after microwaving. This controlled initial drop is essential for locking in the tile geometry and preventing deformation. Once the tile is thermally stabilized, the system transitions to a passive radiative phase, allowing the remaining heat to dissipate gradually into the lunar environment.

### Justification and Performance

This multi-staged configuration provides the necessary thermal shock mitigation to guarantee tile durability without over-engineering the system. By restricting active or conductive elements only to the critical initial phase, the design significantly will reduce the overall power and mass budget compared to a fully active loop. Additionally, this architecture ensures that the payload electronics remain shielded from peak heat loads, maintaining operational reliability throughout repeated manufacturing cycles. This balanced approach ensures high-fidelity tile production while preserving the simplicity required for a successful lunar mission.

### Tile Testing

To determine the success of the tiles, the design will subject them to a series of tests. the design will first leverage the access to a lunar astronaut and use them to collect and return the tiles to Earth, where they can undergo in-depth testing. the design will test for the tile requirements outlined earlier in Figure 5.1. The key measurements the design will need to test for are the impact pressure, the static hold pressure, and the thermal capabilities of the tiles. the design will test for the impact pressure using a drop weight tester. Drop weight testers are a great way to measure impact pressure as long as the impact area is noted. Large drop weight testers are capable of dropping a 2,700 kg object from 4 m. This is more than enough to produce the 424 kPa pressure that the tile must be able to withstand [94]. the design will also use a hydraulic press to determine the

maximum static pressure the tile can withstand to replicate a large lander's weight on the tile, as well as the sustained vertical pressure from the landing plume. A hydraulic press is more than capable of generating the required force. If the design press on the full area of the tile, which is  $0.078 \text{ m}^2$ , the design will need to generate 27,612 kg of force, which is achievable using only a small hydraulic press [95]. This test is key in understanding the static strength of the landing pad tiles. Finally, the design will use an arc jet to test the thermal capabilities of the tile. The arc jet can be used to mimic the plume of a rocket, at least thermally, and thus evaluate the thermal capabilities of the tile. The NASA Ames arc jet is capable of producing 70 MW of power for 30 minutes, which is more than enough to mimic the tile requirement of  $17,786.3 \text{ kW/m}^2$  [96]. These tests will evaluate the basic properties required to render the tile functional as part of a lunar landing pad. Additionally, the design is aware that conducting tests on the lunar surface is important, and the design are working on designing these tests. More on this can be found later in this report under future work.

## 5.6 Communication System

The communication architecture prioritizes low mass and reliability, utilizing the Lander as a relay rather than Direct-to-Earth (DTE) communication. The communication system is an essential part of the mission to relay information from the mission to Earth. The design will use the Griffin lunar lander's communication system to directly relay information from the stationary tile maker and a separate system that will use the lander as a relay for the rover system. The following systems are gone into depth below.

### 5.6.1 Griffin Lunar Lander Communication System

The Griffin lunar lander communication system enables lander commanding and telemetry. The communication system relays information from both the lander itself as well as the payload to Earth. To do this the lander uses a high-powered and flight-heritage transponder, as well as multiple antennas. The lander has multiple low gain antennas to maximize coverage as well as a medium and high gain antenna as well for long distance communication with Earth. The high and low gain antennas can be seen below in a diagram of the lander in figure 5.9. The lander-Earth communication operates in the X-Band frequency range. The connection of the lander and payload is achieved through a Serial RS-422 or SpaceWire for wired communication throughout the mission. This method is reliable and will be viable for the stationary tile maker part of the payload.

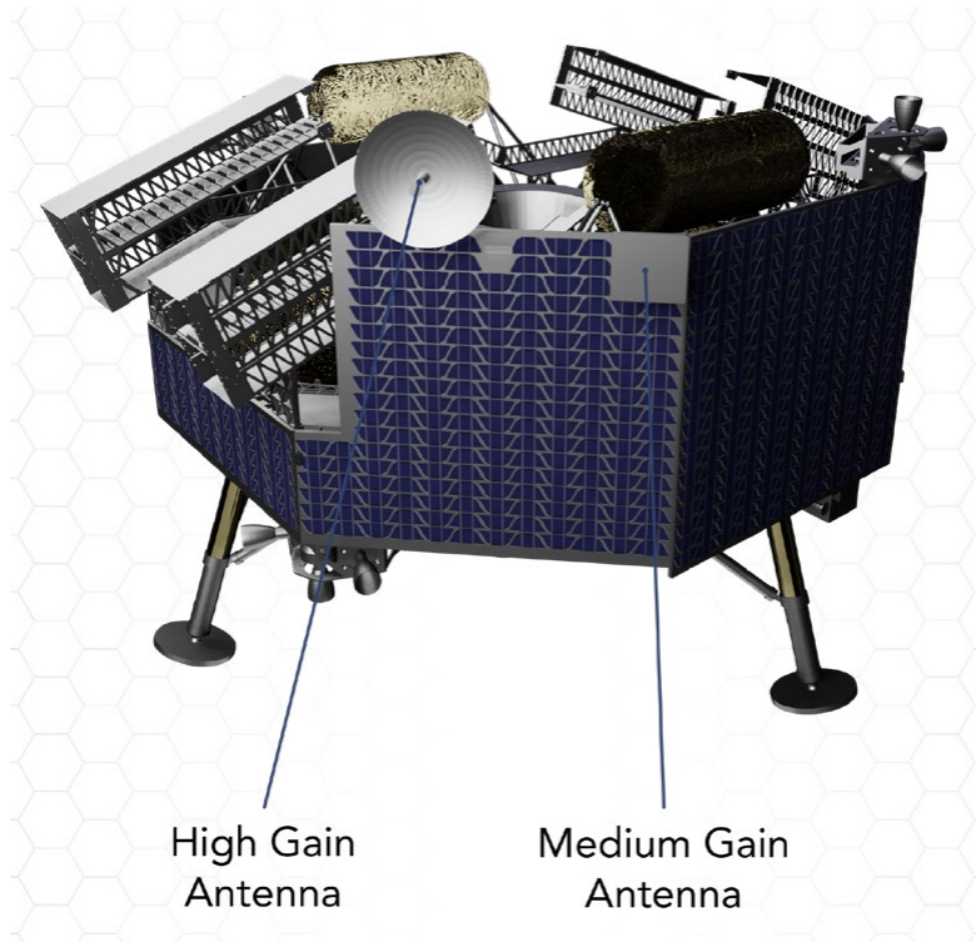


Figure 20: Diagram of the Griffin lunar lander highlighting high and medium gain antennas which allow the lander to communicate to Earth in the X-band [9].

The lander does also have wireless connection capabilities through a 2.4 GHz IEEE 802.11n compliant wire local area network (WLAN) modem. Payloads compatible with 2.4 GHz IEEE 802.11n can communicate with the rover, and the lander relays payload telecommands and telemetry in near real-time. This feature was leveraged for the rover system part of the payload and is discussed more in the next section. The process can be seen in the diagram below produced by Astrobotic. The in-place communication system that the Griffin lunar lander uses is a key part of the mission and heavily relied on.

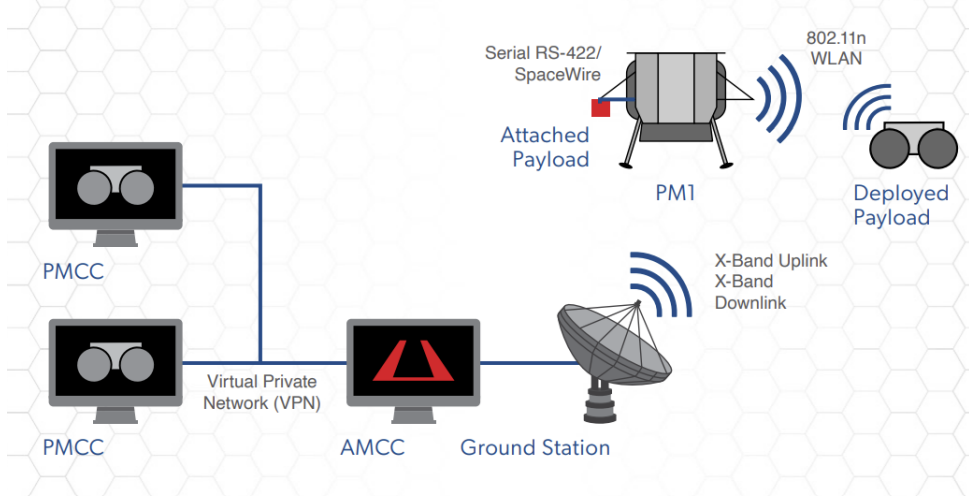


Figure 21: Diagram of communication process between rover, lander, and ground station [9].

### 5.6.2 Rover Communication System

As the rover will completely detach from the Griffin Lunar Lander, it will need a communication system of its own. Establishing a robust and reliable form of communication system for the rover is a fundamental requirement for ensuring the success of the rover and achievement of the goals. The communication system serves as the rover's connection to the rest of the mission as it is deployed. It allows the rover to receive commands from the lander, report its health and status, transmit sensor data, and coordinate the regolith-collection workflow in real time. This link is how the rover stays synchronized with overall mission objectives, updates its tasks as the tile-maker requires more material, and lets operators monitor progress and intervene if needed. In short, without a reliable communication system, the rover cannot safely navigate, cannot deliver materials on demand, and cannot function as an integrated part of the landing-pad construction architecture.

In theory the simplest method of communication is to set up a link directly between the rover and a ground station on Earth. This method while effective and proven, is not without drawbacks. To start, a high-gain antenna is required to relay information all the way to Earth from the moon as the distance between Earth and the moon is so great, approximately 384,000 miles [97]. A high-gain antenna adds both mass and complexity to the communications design. Gain is the term used to describe the antenna's ability to amplify signal power. In essence, how much the antenna can focus the radio beam and in turn the distance it can transmit it. As the radio beam is narrowed, the sweep of directions it covers decreases. This means whenever the rover moves and turns, the high gain signal runs the risk missing Earth [98]. Additionally, high gain antennas in general have more mass than low gain antennas as larger parabolic dishes are good at focusing radio beams are great high gain antennas. [99]. For example the NASA Perseverance rover uses a high gain antenna system that weighs approximately 8 kg [100]. The rover is simply too small to handle the complexities as well as mass concerns that using a high gain antenna would cause.

Luckily, as mentioned before, the Griffin lunar lander can serve as relay between the rover and Earth. This is significant because it allows for the use of low-gain antennas, which do not have the distance range to send radio waves to Earth. The Griffin lunar lander uses a 2.4 GHz IEEE 802.11n compliant WLAN modem to connect with deployable payloads wirelessly [9]. This narrows down the options on communication systems as the design must be compatible with the Griffin lunar lander modem.

To start, the design will use a WGM160P module to establish the rover's primary wireless communications link with the lander. This module provides a compact and low-power Wi-Fi radio that interfaces directly with the rover's onboard computer to maintain a continuous data link with the Griffin lander [101]. Additionally,

power to the module will be conditioned through regulated and filtered electronics. These electronics will not be able to handle the lunar environment on their own and hence will be kept in an electronics box to protect them. The design will also use insulation methods discussed later in this section.

For the antennas, the design will use two 2.4 GHz Pagoda antennas. While the distance range is lower for these antennas than a high-gain or medium-gain antenna, the rover will not travel very far from the Griffin lunar lander at all, making it so that the antennas do not need to have a great distance range. These low-gain antennas have a gain of 0.6 to 1.3 dBi, which is very low and will ensure a wider range of coverage, which also reduces complexity in how the design orients the antennas. The wide range of these antennas can be seen in Figure 22 below, which compares the ranges of different dBi (the measurement of gain) antennas. These antennas are also built for lunar communications and are compatible with the 2.4 GHz IEEE 802.11n WLAN modem and thus will work with the communication architecture. The design will use two on opposite sides of the rover to ensure full coverage as well as add redundancy to the system in the case that one is damaged. This is a common practice for space crafts [98].

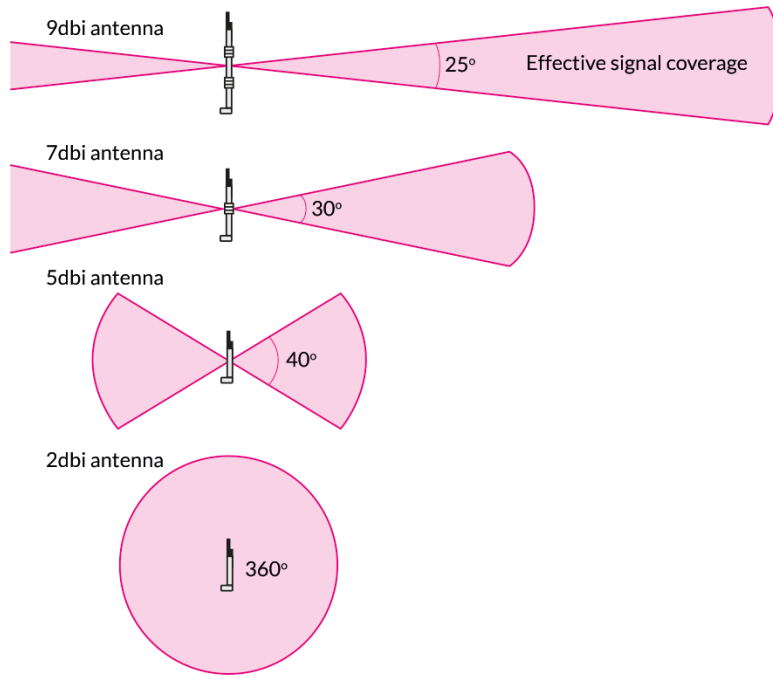


Figure 22: Depiction of the range for antennas based on their dBi (low gain 0 - 3 dBi, medium gain 3 - 8 dBi, high gain 9 - 15 dBi) [102].

Finally, the design will need to have an insulation system for these electronics, as they are not all designed to survive on the moon. Extreme temperature and temperature swings, as well as radiation from the sun, are among the biggest concerns for these electronics. For this reason, the design will use multilayer insulation, or MLI. The MLI will consist of aluminized Kapton, Kapton, Mylar, and aerogel. This layered architecture is designed to combat radiation, thermal, and dust concerns. The aluminized Kapton is reflective and can reflect thermal radiation from the sun that would otherwise damage the electronics. It is also functional between  $-250^{\circ}\text{C}$  to  $290^{\circ}\text{C}$ , which encompasses all the temperatures on the lunar surface [103]. Kapton laminate has a very low absorptance of under 0.14, which means it does not heat up as much under the sun. It also has a very low emittance of under 0.04, meaning heat loss is also slowed for the cold lunar nights [104]. This combination yields Kapton a fantastic way of regulating the extreme temperatures experienced on the moon. Finally, the design will use aerogel layers in the MLI. Aerogel is extremely resilient to low and high temperatures, up to

1100°C, incredibly light as it is mostly air, and has very low thermal conductivity, which makes it a great insulation material. In the past, it has been too brittle however, advancements in the technology have made it more flexible and stronger. Aerogel is about one-third the mass of state-of-the-art insulation materials [105]. There is no doubt that aerogel is the future of spacecraft aviation and will serve the insulation requirements well. These materials will be layered together with the aluminized Kapton on the outside, as it is reflective, and the aerogel on the inside, as it is still the most fragile of the materials. There will be approximately 10 to 20 layers, only accumulating to a few millimeters thick, as this is standard [106].

Our rover communication system is designed to be lightweight, effective over short ranges, robust, and environmentally protected. The design will accomplish this using the Griffin lunar lander as a relay, a Wi-Fi module, low-gain antennas, and MLI of proven materials. The low mass of each chosen component is crucial, as the weight of the rover is so small. The relay capabilities of the Griffin lunar lander open the door for the use of lower distance range antennas, which is also a large factor in keeping the mass low. This communication system will help transmit and receive critical information from the rover as it gathers regolith for the construction of tiles.

## 6 Architecture Analysis

### 6.1 Mass Budget

The mass budget for the system was developed using a bottom-up estimation approach. Unlike early stage conceptual designs that rely on historical percentages, this budget utilizes mass values for specific sub components identified during the preliminary design phase. This includes distinct estimates for the rover mobility platform and the tile maker processing system. This approach was applied to all major subsystems, including Structural, Power, Microwave Sintering, and Processing. To account for uncertainty in the design maturity of specific components, growth allowances were applied to each line item. These allowances adhere to standard AIAA mass growth guidelines, ranging from 10% components to 30% or higher for detailed elements.

Table 22: Mass Budget with Growth Allowance.

Main Subsystems	Component	Mass (kg)	Growth Allowance	Growth (kg)	Total Mass (kg)
<b>1.0 Structural &amp; Mechanical</b>	Rover: Chassis & Frame	4	0.15	0.6	4.6
	Rover: Wheels (4x Rigid Al)	1.8	0.1	0.18	1.98
	Rover: Excavation Arm	3	0.2	0.6	3.6
	Rover: Hopper Structure/Mech	2.8	0.15	0.42	3.22
	Tile Maker: Chassis & Frame	30	0.25	7.5	37.5
	Tile Maker: Reception Hopper	6	0.25	1.5	7.5
	Tile Maker: Telescoping Ramp	6	0.25	1.5	7.5
	Tile Maker: Frame/Support	15	0.3	4.95	19.95
Structural Subtotal					<b>85.85</b>
<b>2.0 Power</b>	Rover: Battery Pack (500Wh)	3	0.1	0.3	3.3
	Rover: Solar Panels	1	0.1	0.1	1.1
	Power Harness/Cables	20	0.2	-	-
	Tile Maker: PDU/Regulation	TBD	0.2	-	-
	Power Subtotal				<b>24.4</b>
<b>3.0 Microwave Sintering</b>	Solid-state low-power generator	30	0.15	4.5	34.5
	Phase Array Antenna	10	0.15	1.5	11.5
	Sintering Subtotal				<b>46</b>

Table 23: Table 22 Continued.

Main Subsystems	Component	Mass (kg)	Growth Allowance	Growth (kg)	Total Mass (kg)
<b>4.0 Thermal</b>	Rover: Thermal/Dust Protection	1.5	0.25	0.38	1.88
	Tile Maker: Ceramic Fiber Insulation	TBD	0.3	—	—
	Tile Maker: Thermal Sink Plates	TBD	0.25	—	—
	<b>Thermal Subtotal</b>				<b>1.88</b>
<b>5.0 Comm &amp; CDH</b>	Rover: Main Computer	0.3	0.1	0.03	0.33
	Rover: Nav Sensors/IMU	0.5	0.15	0.05	0.55
	Rover: Comms (Antenna + Transceiver)	0.3	0.15	0.05	0.35
	Tile Maker: Sensors (Temp/Mass)	TBD	0.2	—	—
	<b>Comm/CDH Subtotal</b>				<b>1.23</b>
<b>6.0 Payload/Processing</b>	Rover: Drive Motors (x4)	2	0.15	0.3	2.3
	Tile Maker: Vibratory Screen Assembly	12	0.3	3.6	15.6
	Tile Maker: Weigh Bin System	5	0.25	1.25	6.25
	Tile Maker: Microwave Sintering Unit	TBD	0.4	—	—
	<b>Payload/Processing Subtotal</b>				<b>24.15</b>
<b>Sum of Totals</b>					<b>183.51</b>

This estimation results in a total projected system mass of 183.51 kg, as detailed in Table 22 and Table 23. The primary mass driver for the mission is the Structural & Mechanical subsystem (85.85 kg), which accounts for the heavy-duty chassis required to support the regolith processing hardware. The second largest contributor is the Microwave Sintering subsystem (46.0 kg), driven by the 30 kg solid-state generator and phase array antenna required to achieve the necessary thermal output for tile production.

The budget also highlights the distinction between the mobility platform and the processing infrastructure. The tile maker chassis and support frame (combined 57.45 kg with growth) is significantly heavier than the rover mobility chassis (4.6 kg), reflecting the stationary stability required during the sintering process. While specific cabling and thermal plate masses remain to be determined, conservative growth allowances have been allocated in the Thermal and Power subsystems to prevent budget overruns as the design matures.

## 6.2 Power Budget

The power budget provided by the Griffin lander is 5 kW as stated in the RFP [3]. The following power budget tables are estimates of the entire power used for both the rover and the stationary tile factory. Better estimates will be chosen and calculated with our specific electronics and parts that will be chosen next semester.

Table 24: Power Draw by Operating Mode for Stationary Tile Factory.

Mode	Description	Power Draw
Conditioning	Vibratory methods & Release methods	250 W
Sintering	1 kW RF for microwave as well as added draw from Press and Controls	1.5 kW
Ejecting Bricks	Move finished bricks off the factory line	0.4 kW
Idle	Day: electronics ready & Night: survival heat & communications	50 W (day), < 10 W (night)

Table 25: Rover Power Usage Summary.

Mode	Description	Power Draw
Controls	Driving, Dumping, & Communications	< 200 W
Digging & Scoop	Collecting regolith	< 150 W
Total Battery Capacity	Sufficient for a full day with multiple trips	480 Wh

### 6.3 Cost Analysis

Table 26: Subsystem and Component Cost Estimates for Rover & Tile Maker.

Main Subsystems	Component	Cost Estimate
<b>1.0 Structural &amp; Mechanical</b>		
	Rover: Chassis & Frame	\$50,000
	Rover: Wheels (4x Rigid Al)	\$30,000
	Rover: Excavation Arm	\$600,000
	Rover: Hopper Structure/Mech	\$45,000
	Tile Maker: Reception Hopper	\$50,000
	Tile Maker: Telescoping Ramp	\$15,000
	Tile Maker: Frame/Support	\$100,000
	<b>Total:</b>	<b>\$890,000</b>
<b>2.0 Power</b>		
	Rover: Battery Pack (500Wh)	\$70,000
	Tile Maker: Power Harness/Cables	\$7,500
	Tile Maker: PDU/Regulation	\$50,000
	<b>Total:</b>	<b>\$127,500</b>
<b>3.0 Thermal</b>		
	Rover: Thermal/Dust Protection	\$200,000
	Tile Maker: Ceramic Fiber Insulation	\$40,000
	Tile Maker: Thermal Sink Plates	\$40,000
	<b>Total:</b>	<b>\$280,000</b>
<b>4.0 Comm &amp; CDH</b>		
	Rover: Main Computer	\$350,000
	Rover: Nav Sensors/IMU	\$75,000
	Rover: Comms (Antenna + Transceiver)	\$60,000
	Tile Maker: Sensors (Temp/Mass)	\$15,000
	<b>Total:</b>	<b>\$500,000</b>
<b>5.0 Payload/Processing</b>		
	Rover: Drive Motors (x4)	\$60,000
	Tile Maker: Vibratory Screen Assembly	\$30,000
	Tile Maker: Weigh Bin System	\$35,000
	Tile Maker: Microwave Sintering Unit	\$100,000
	<b>Total:</b>	<b>\$225,000</b>
	<b>Complete Total:</b>	<b>\$2,022,000</b>

Above is the preliminary cost estimates for each system in the tile maker and rover. These estimates in the future are subject to change.

## 6.4 Risk Analysis

The risks for this mission are quantified by two criteria: the consequence of failure and the likelihood of said risk occurring. Each criterion is assessed on a scale from 1 to 5, with higher values indicating more severe consequences or greater probability of occurrence. The qualitative definitions for each level of consequence and likelihood are provided in Table 27.

Table 27: Risk Level Definition.

Consequence of Failure		Likelihood of Failure	
<b>Catastrophic (5)</b>	Mission fails to produce landing pad, and any technical demonstrations.	<b>Very High (5)</b>	81% – 100%
<b>Critical (4)</b>	Mission fails to demonstrate capability of landing pad, few results collected.	<b>High (4)</b>	61% – 80%
<b>Moderate (3)</b>	Mission experiences reduced performance in one of mission critical systems.	<b>Medium (3)</b>	41% – 60%
<b>Minor (2)</b>	Mission experiences reduced performance affecting one of the noncritical systems.	<b>Low (2)</b>	21% – 40%
<b>Negligible (1)</b>	Mission requires slight changes after launch.	<b>Very Low (1)</b>	0% – 20%

In addition, risks have also been categorized into six categories: Mass (M), General (G), Environmental (E), Power (P), Schedule (Sc), and Structural (St). These categories can be seen clearly in Table 28.

Table 28: Risk Classification Legend.

Risk Classification	Category
M	Mass
G	General
E	Environmental
P	Power
Sc	Schedule
St	Structural

A series of high-level risks relevant to the mission have been identified. These are risks that if they are not addressed, could impact mission performance, the schedule, or overall safety. As the design progresses, each risk will need to be monitored, updated, and reassessed. Table 29 summarizes the current mission-level risks, showing their initial consequence and likelihood, the mitigation strategy proposed, and the expected risk levels after mitigation.

Each risk from Table 29 is visualized in Figure 23 using a risk matrix. In this matrix, the arrows represent risk level after mitigation methods are applied. The figure highlights three levels that a risk may fall into: green being acceptable, yellow being moderate, and red being critical. At this early stage of the design, several risks fall into moderate or even critical zones such as change in regolith composition at the landing site (G2) or surpassing available mass limit (M1). As the design becomes more refined and mitigation measures are

implemented, these risks are expected to shift toward lower-risk regions. The projected post-mitigation values are listed in Table 29 and shown through the arrows in Figure 23.

Table 29: High Level Mission Risks and Mitigation Outcomes.

Risk ID	Risk Statement	Consequence	Likelihood	Mitigation	Consequence After Mitigation	Likelihood After Mitigation
M1	Surpassing available mass	5	3	Use conservative mass estimates	5	1
Sc1	Schedule overrun	2	4	Use conservative time estimates and budget accordingly	1	4
G1	Solar panels dust accumulation	3	3	Controlled dumping of regolith and dust shield	3	1
P1	Unexpectedly low microwave efficiency	2	4	Extensive testing beforehand	2	1
St1	Rover is unable to traverse terrain and gets stuck	5	2	Choose a flat landing/collecting site	5	1
G2	Change in regolith composition at the landing site	4	4	Choose a location with stable and predictable regolith	4	2
E1	Radiation overheats microwave unit	4	3	Implement a cooling system	2	3

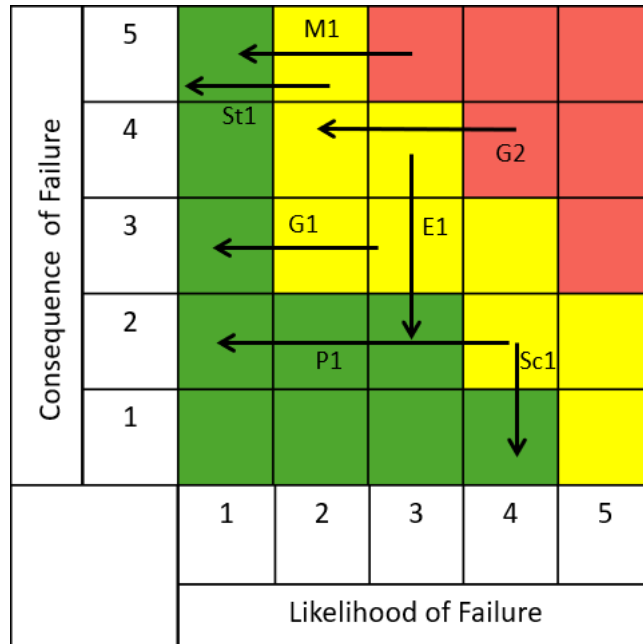


Figure 23: Risk Matrix detailing the likelihood and consequence of failure before and after mitigation.

Taken together, the results shown in Table 29 and Figure 23 suggest that, once mitigation is applied, most of the evaluated items fall within the green area of the matrix. In practical terms, this means they are acceptable for the current stage of the mission. Although some uncertainty is unavoidable at this point in the design, the overall trend shows that the mitigation measures proposed so far are working as intended and are effective in bringing potential issues down to manageable levels.

## 6.5 Future Work

VT Luna's current goal is a proof of concept, saying that tiles can be made on the Moon. In the future VT LUNA want a full tile factory, building a fully usable landing pad. To do this, future work that VT Luna hopes to explore includes the following:

### 6.5.1 Rover Autonomy and Terra-forming

Enhancing rover autonomy. Currently, the rover is designed primarily to support regolith collection and regolith delivery, but a future iteration will incorporate expanded navigation, perception, and manipulation capabilities. This would enable the rover not only to collect and transport regolith but also to relocate completed tiles from the stationary tile maker to a designated testing or staging area. In order to create the landing pad the construction area needs to be properly leveled and terraformed. Improvements to the scoop design and autonomy will allow the rover to prepare the construction area on its own. Investigating the feasibility and reliability of such autonomous tile-handling and ground leveling operations will be critical for reducing human oversight and enabling scalable surface construction.

### 6.5.2 Tile Testing

Another research direction involves the development of robust, repeatable tile testing methods that can be conducted directly on the lunar surface. While returning tiles to Earth provides valuable insights into microstructure and mechanical performance, it is neither scalable nor cost-effective for long-term operations. Establishing

on-site test procedures, such as compressive strength evaluation, thermal cycling exposure, and dust abrasion testing, would provide immediate, mission-relevant data and accelerate the iterative design process.

### **6.5.3 Finite Element Analysis**

Finite Element Analysis of a variety of tile designs under different loading conditions such as the landing of a SpaceX Starship HLS. Finite Element Analysis will play a central role in optimizing future tile designs. By modeling various geometries, material distributions, and interlocking mechanisms under realistic loading conditions, the team can identify configurations that offer improved durability, thermal stability, and load-bearing performance. These simulations will guide the refinement of both the sintering process and the structural layout of the tiles.

### **6.5.4 Interlocking Tile Designs**

If constraints in the manufacturing process are overcome, designs with interlocking geometry could be employed. Interlocking tiles would be valuable as they allow for the distribution of lateral forces between tiles, multiple layers of tiles to be stacked on top of each other as reinforcement, and mitigates the chances of tiles being ejected by the plume of landing rockets.

Before radial shrinkage of the tiles was acknowledged during the sintering and cooling process, the tile design was based upon the hexagonal design but incorporating dovetail joints. These dovetail joints allow tiles to "transfer increasing loading with no sudden failure" and "this type of behavior is suitable especially in terms of safety of the construction" [107]. Therefore, if the constraints of material shrinkage are able to overcome through post-processing causing RTR 2.2, implementing this sort of design would be a major improvement over the current design.

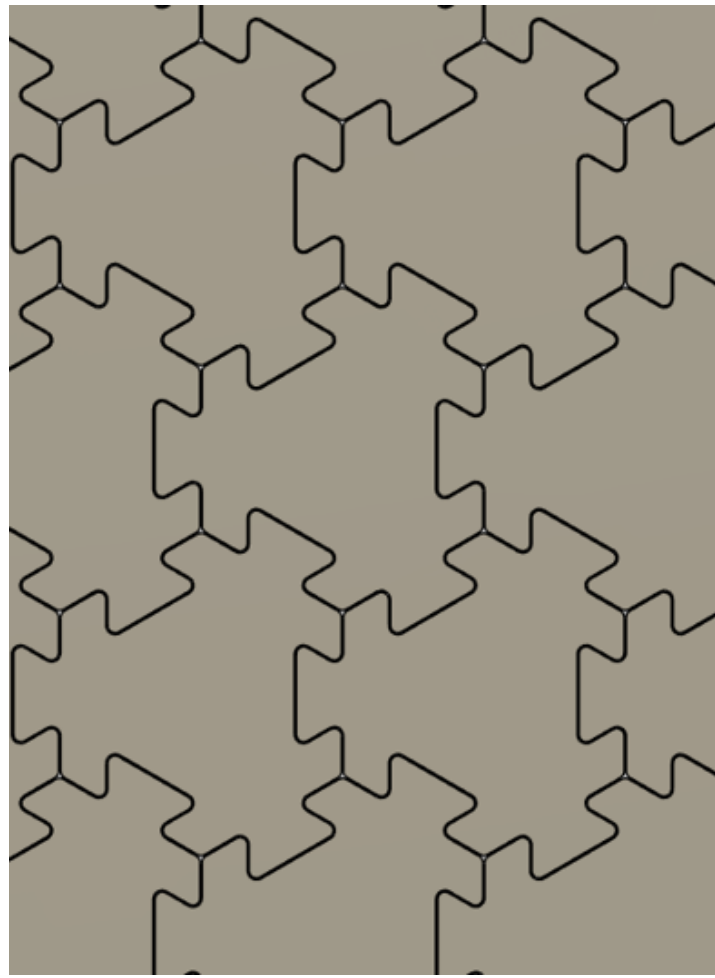


Figure 24: Image of the dovetailed tile design highlighting how the tiles interlock with each other to transfer loads.

The preexisting tile design was also found, which incorporates a vertical interlocking design. This design allows for "Stacking multiple layers of tiles instead increases the structure's reliability... allowing for redundancy and rapid repairs" [32]. While this concept is unique and has advantage, the requirements of the compression and sintering process causing RTR 2.1 would have to change significantly to produce this design or utilize a similar concept.

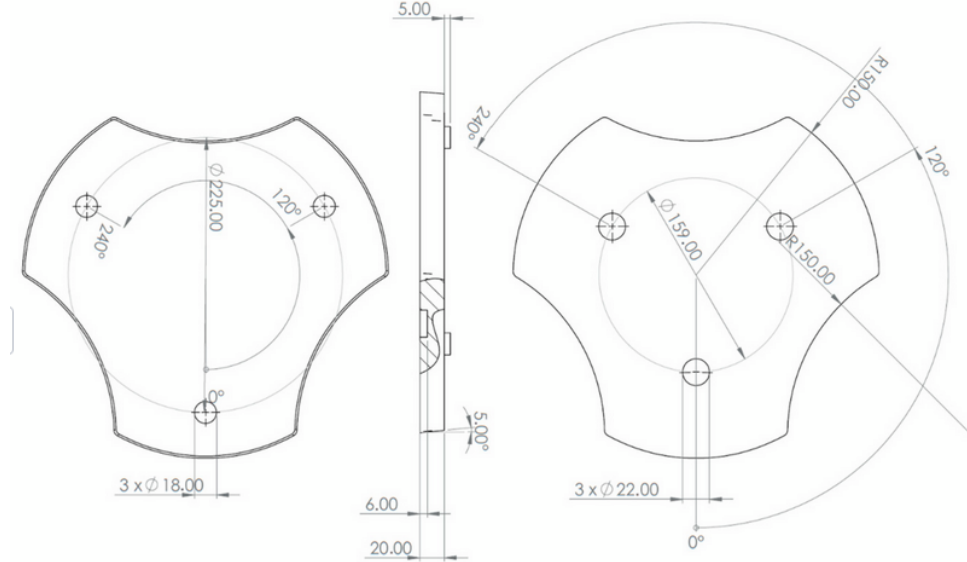


Figure 25: Technical drawing of the vertically interlocking tile design showing that a lack of vertical homogeneity allows for tiles to interface with each other in the out of plane dimension [32].

## 6.6 Conclusion

The VT LUNA design proposes a scalable, autonomous solution for lunar infrastructure. Lunar landing pads will be constructed as they are a crucial piece of initial lunar architecture. The design for this construction revolves around a stationary tile maker and a lunar regolith collection rover. The stationary tile makes landing pad tiles by layering lunar regolith and sintering it repeatedly. The design is a proof of concept as it will be unable to create enough tiles for a full landing pad. However, the concept is extremely scalable with higher power access and an increased number of tile makers. By leveraging a separate collection rover and a stationary microwave sintering factory, the system minimizes mass while maximizing throughput. Future work will focus on refining the power model for sintering, conducting structural integration of the rover arm, and finalizing the specific "dock-to-charge" interface mechanisms.

# Bibliography

- [1] “Artemis,” Accessed 2025-12-10.
- [2] “CosmicSpace.org,” Homepage, accessed 2025-12-10.
- [3] “C3 — CosmicSpace.org,” Accessed 2025-12-10.
- [4] National Aeronautics and Space Administration, “Apollo Lunar Surface Journal — Historical Technical Memo TM-2005-213610,” Technical Memorandum TM-2005-213610, NASA, 2005, Accessed 2025-12-10.
- [5] NASA, “Lander Plume Ejecta — Experimental and Numerical Results,” Technical Report NASA / TM-2020-503590, NASA, 2020, Accessed 2025-12-10.
- [6] Mueller, R. P., “Lunar Landing & Launch Pads,” 2020, Accessed 2025-12-10.
- [7] National Aeronautics and Space Administration (NASA), “Artemis: Humans in Space,” NASA Website, 2025.
- [8] “Astrobotic.com,” Homepage, accessed 2025-12-10.
- [9] Astrobotic Technology, Inc., “Astrobotic Lunar Landers: Payload User’s Guide,” Tech. Rep. Version 5.02, Astrobotic Technology, 2021.
- [10] Giwa, I. et al., “3D Printed Sulfur-Regolith Concrete Performance Evaluation,” *Construction and Building Materials*, 2024, Study on sulfur binder concrete for lunar construction.
- [11] Lim, S. et al., “Investigating the microwave heating behaviour of lunar soil,” *Scientific Reports*, Vol. 11, 2021, pp. 1–12, Shows microwave heating as more viable than solar sintering for regolith processing.
- [12] Bryant, S., “Lunar Pole Illumination and Communications Maps Computed from Goldstone Solar System Radar Elevation Data,” Interplanetary Network Progress Report 42-176, Jet Propulsion Laboratory, California Institute of Technology, February 2009, Accessed 2025-12-10.
- [13] “NASA Identifies Candidate Regions for Landing Next Americans on the Moon,” 2024, Accessed 2025-12-10.
- [14] “NASA Provides Update on Artemis III Moon Landing Regions,” 2022, Accessed 2025-12-10.
- [15] European Space Agency, “Microwave Heating of Lunar Regolith (Microlith),” <https://www.youtube.com/watch?v=4WguxZ100-U>, 2025, YouTube video, accessed 12 December 2025.
- [16] NASA Goddard Space Flight Center, “Lunar Topographic Map from First 1 Billion LOLA Measurements,” NASA Lunar Reconnaissance Orbiter (LRO) / LOLA data, 2010–2011, Derived from LOLA altimetry data, accessed 12 December 2025.

- [17] Lee, H., Jun, S., Kim, J., Kim, D., Lee, S., and Park, J., "Microwave Sintering of Lunar Soil Simulant for In-Situ Resource Utilization," *Scientific Reports*, Vol. 11, 2021, pp. 791, accessed 12 December 2025.
- [18] of the paper, A., "Title of the Article," *Scientific Reports*, Vol. 14, 2024, pp. 79504, accessed 12 December 2025.
- [19] European Space Agency, "Microwave Heating and Sintering of Lunar Regolith," <https://www.youtube.com/watch?v=-ZI8e82ZEv0>, 2025, YouTube video, accessed 15 November 2025.
- [20] Rumble, J. R., editor, *CRC Handbook of Chemistry and Physics*, CRC Press, Boca Raton, FL, 104th ed., 2023, Thermophysical properties of inorganic compounds, including refractory oxides.
- [21] Strangway, D. W., Pearce, G. W., and Olhoeft, G. R., "Magnetic and Dielectric Properties of Lunar Samples," *Proceedings of the Soviet-American Conference on Cosmochemistry of the Moon and Planets, Part 1*, NASA, Washington, DC, 1977, NASA Technical Reports Server (NTRS) Document ID: 19780005009.
- [22] European Space Agency, "Microwaves Heating and Sintering of Regolith (Microlith)," <https://nebula.esa.int/content/microwaves-heating-sintering-regolith-microlith>, 2025, ESA Nebula article, accessed 12 December 2025.
- [23] European Space Agency, "Microwave Heating of ISRU Feedstock," <https://nebula.esa.int/content/microwave-heating-isru-feedstock>, 2025, ESA Nebula article, accessed 12 December 2025.
- [24] Watson-Morgan, L., Hawkins, L., Crisler, J., Gagliano, L., Ortega, R., Percy, T. K., Polsgrove, T., and Vermette, J., "NASA's Initial Artemis Human Landing System," *73rd International Astronautical Congress (IAC)*, International Astronautical Federation (IAF), Paris, France, September 18–22 2022, Document ID 20220013431, available from NASA Technical Reports Server.
- [25] Jehn, I. E. and Dreyer, C. B., "A design methodology for flat slab lunar landing and launch pad systems," *Acta Astronautica*, Vol. 231, 2025, pp. 175–192.
- [26] Indyk, S. J. et al., "A structural assessment of unrefined sintered lunar regolith," *Acta Astronautica*, Vol. 139, 2017, pp. 353–362.
- [27] Warren, P., Raju, N., Ebrahimi, H., Krsmanovic, M., Raghavan, S., Kapat, J., and Ghosh, R., "Effect of Sintering Temperature on Microstructure and Mechanical Properties of Molded Martian and Lunar Regolith," *Ceramics International*, Vol. 48, No. 23, 2022, pp. 35825–35833.
- [28] Kim, Y.-J., Ryu, B.-H., Jin, H., Lee, J., and Shin, H.-S., "Microstructural, mechanical, and thermal properties of microwave-sintered KLS-1 lunar regolith simulant," *Ceramics International*, Vol. 47, No. 19, 2021, pp. 26891–26897.
- [29] Farries, K. W., Visintin, P., Smith, S. T., and van Eyk, P., "Sintered or melted regolith for lunar construction: state-of-the-art review and future research directions," *Construction and Building Materials*, Vol. 296, 2021, pp. 123627.
- [30] Han, W., Zhou, Y., Cai, L., Zhou, C., and Ding, L., "Physical, Mechanical and Thermal Properties of Vacuum Sintered HUST-1 Lunar Regolith Simulant," *International Journal of Mining Science and Technology*, Vol. 34, 2024, pp. 1243–1257.
- [31] Air Force Flight Dynamics Laboratory, "Analysis of Plates in Bending," <https://engineeringlibrary.org/reference/analysis-of-plates-bending-air-force-stress-manual>, 1986, Chapter from the Stress Analysis Manual.

- [32] Pastore, A., Agozzino, M., and Ferro, C. G., “A Lunar Landing Pad from IRSU Materials: Design and Validation of a Structural Element,” *Aerospace*, Vol. 12, No. 9, 2025, pp. 781.
- [33] Olhoeft, G. R., “Lunar Sample Electrical Properties,” *Lunar and Planetary Science Conference Proceedings*, 1973, Presented at the 1973 Lunar and Planetary Science Conference.
- [34] Taylor, L. A. and Meek, T. T., “Microwave Sintering of Lunar Soil: Properties, Theory, and Practice,” *Journal of Aerospace Engineering*, Vol. 18, No. 3, 2005, pp. 188–196.
- [35] Kost, P.-M., Linke, S., Gundlach, B., Lethuillier, A., Baasch, J., Stoll, J., and Blum, J., “Thermal properties of lunar regolith simulant melting specimens,” *Acta Astronautica*, Vol. 187, 2021, pp. 429–437.
- [36] Bassett, H. L., “Dielectric properties of Apollo 14 lunar samples at microwave frequencies,” *Lunar and Planetary Science Conference Proceedings*, 1972, Presented at the 1972 Lunar and Planetary Science Conference.
- [37] “Automeris.io — Interactive data visualization tools,” <https://automeris.io/>, 2025, Accessed: 2025-12-12.
- [38] Department, M. E., “Introduction to Robotics,” <https://me.berkeley.edu/academics/courses/introduction-to-robotics/>, Accessed: 2025-01-01.
- [39] LLC, H. D., “Articulated Arm Joint Torque Calculations,” <https://www.harmonicdrive.net/>.
- [40] Inc., G., “DC Planetary Gearmotors for Efficiency and High Torque,” <https://www.groschopp.com/dc-planetary-gear-motors/>, Accessed: 2025-01-01.
- [41] Inc., A., “AndyMark Robotics Components,” <https://www.andymark.com/>, Accessed: 2025-01-01.
- [42] Mabuchi Motor Co., L., “Mabuchi Motor Product Information,” <https://product.mabuchi-motor.com/>, Accessed: 2025-01-01.
- [43] RobotShop, “RobotShop: Robotics Parts, Motors, and Components,” <https://www.robotshop.com/>, Accessed: 2025-01-01.
- [44] Supply, G. I., “Grainger MRO Products, Tools, and Industrial Equipment,” <https://www.grainger.com/>, Accessed: 2025-01-01.
- [45] NASA, “NASA Homepage and Mission Resources,” <https://www.nasa.gov/>, Accessed: 2025-01-01.
- [46] Johnson, T. and Engineers, N., “Lunar and Planetary Mobility Systems: Technical Report TP-202510470,” <https://ntrs.nasa.gov/api/citations/20250010470/downloads/Johnson%20TP-202510470.pdf>, NASA Technical Reports Server, Accessed: 2025-01-01.
- [47] Zhang, X. et al., *Terramechanics and Off-Road Vehicle Engineering*, Wiley, 2021, Accessed: 2025-01-01.
- [48] NASA, “Mars Exploration,” <https://mars.nasa.gov/>, Accessed: 2025-01-01.
- [49] Thrun, S., Burgard, W., and Fox, D., *Probabilistic Robotics*, MIT Press, 2005.
- [50] Foundation, O. S. R., “ROS Navigation Stack Documentation,” <https://www.ros.org/>, Accessed: 2025-01-01.
- [51] Nister, D., Naroditsky, O., and Bergen, J., “Visual Odometry Tutorial,” *IEEE Journals & Magazines*, 2004, Accessed: 2025-01-01.

- [52] Durrant-Whyte, H. and Bailey, T., “Simultaneous Localization and Mapping: Part I,” *IEEE Robotics & Automation Magazine*, 2006, Accessed: 2025-01-01.
- [53] NASA, “Mars - NASA Science,” <https://science.nasa.gov/mars/>, Accessed: 2025-01-01.
- [54] Ouster, “VLP-16 LiDAR Specifications,” <https://ouster.com/products/vlp-16/>, Accessed: 2025-01-01.
- [55] Liu, X. et al., “Fusion-Odometry-Based Global Navigation in Closed Orchards,” *Journal of Field Robotics*, 2020, Accessed: 2025-01-01.
- [56] Laboratory, N. J. P., “JPL Robotics,” <https://robotics.jpl.nasa.gov/>, Accessed: 2025-01-01.
- [57] International, A., “ASM Handbook: Materials and Processing,” <https://www.asminternational.org/>, Accessed 2025-01-01.
- [58] OnlineMetals, “Aluminum Material Data and Properties,” <https://www.onlinemetals.com/>, Accessed 2025-01-01.
- [59] Explorers, N. . H., “HELEX: Solar Orbiter and Sentinels Report,” <https://ntrs.nasa.gov/>, Accessed 2025-01-01.
- [60] NASA, “Lunar Dust Effects on Materials,” <https://ntrs.nasa.gov/citations/20130009098>, Accessed 2025-01-01.
- [61] International, A., “ASM Handbook: Stainless Steels,” <https://www.asminternational.org/>, Accessed 2025-01-01.
- [62] MatWeb, “Titanium Alloys - Ti6Al4V Grade 5 Material Data,” <https://www.matweb.com/>, Accessed 2025-01-01.
- [63] AZoM, “Troublesome Titanium – Machining This Tough Material,” <https://www.azom.com/article.aspx?ArticleID=1547>, Accessed 2025-01-01.
- [64] Coromant, S., “Tips on Machining Titanium Alloys,” <https://www.sandvik.coromant.com/>, Accessed 2025-01-01.
- [65] Oberg and Others, “Machinery’s Handbook,” <https://ntrs.nasa.gov/citations/20080032587>, Accessed 2025-01-01.
- [66] Battery, K., “24V 20Ah Deep Cycle Lithium LiFePO4 Battery,” <https://www.keheng-battery.com>, Accessed 2025-01-01.
- [67] NVIDIA, “Jetson Orin Nano Power Range (7–15 W),” <https://developer.nvidia.com/embedded>, Accessed: 2025-01-01.
- [68] CpuTronic, “NVIDIA Jetson Orin Nano 8 GB: Detailed Specifications and Benchmark Ratings,” <https://www.cputronic.com/jetson-orin-nano-specifications>, Accessed: 2025-01-01.
- [69] STMicroelectronics, “STM32 Nucleo Boards,” <https://www.st.com/en/evaluation-tools/stm32-nucleo-boards.html>, Accessed: 2025-01-01.
- [70] PJRC, “Teensy 4.1 Power Consumption and Specifications,” <https://www.pjrc.com/store/teensy41.html>, Accessed: 2025-01-01.

- [71] STMicroelectronics, “Our Technology Starts With You,” [https://www.st.com/content/st\\_com/en/about/our-technology.html](https://www.st.com/content/st_com/en/about/our-technology.html), Accessed: 2025-01-01.
- [72] International, D., “XBee-PRO 900HP/XSC RF Modules Datasheet,” [https://www.digi.com/resources/documentation/digidocs/pdfs/ds\\_xbee-pro-900hp.pdf](https://www.digi.com/resources/documentation/digidocs/pdfs/ds_xbee-pro-900hp.pdf), Accessed: 2025-01-01.
- [73] Foundation, R. P., “Buy a Raspberry Pi Camera Module 2,” <https://www.raspberrypi.com/products/camera-module-2/>, Accessed: 2025-01-01.
- [74] RealSense, I., “Intel RealSense LiDAR Camera L515 Datasheet,” <https://www.intelrealsense.com/l515-lidar-camera/>, Accessed: 2025-01-01.
- [75] Motor, B. G., “Gear Motor Selection Guide: How to Choose High Torque Gear Motors,” <https://bestgarmacotor.com/how-to-choose-high-torque-gear-motor/>, Accessed: 2025-01-01.
- [76] AutomationDirect, “Electric Motors — Industrial Motors,” <https://www.automationdirect.com>, Accessed: 2025-01-01.
- [77] NVIDIA, “Jetson Orin Nano Developer Resources,” <https://developer.nvidia.com>, Accessed: 2025-01-01.
- [78] STMicroelectronics, “STMicroelectronics Official Website,” <https://www.st.com>, Accessed: 2025-01-01.
- [79] PJRC, “Teensy 4.1 Microcontroller Board,” <https://www.pjrc.com/store/teensy41.html>, Accessed: 2025-01-01.
- [80] Electronics, P. R. ., “Brushed DC Motor Controllers,” <https://www.pololu.com/category/10/brushed-dc-motor-controllers>, Accessed: 2025-01-01.
- [81] ROS, O. R. ., “Nav2 Navigation Stack Documentation,” <https://navigation.ros.org>, Accessed: 2025-01-01.
- [82] Arduino, “Arduino Official Store,” <https://store.arduino.cc>, Accessed: 2025-01-01.
- [83] Industries, A., “INA219 Current Sensor Breakout Guide,” <https://learn.adafruit.com/adafruit-ina219-current-sensor-breakout>, Accessed: 2025-01-01.
- [84] Instruments, T., “Battery Management ICs,” <https://www.ti.com/power-management/battery-management/overview.html>, Accessed: 2025-01-01.
- [85] Kleinhans, M. G. et al., “Vacuum Effects on Lunar Soil Simulants: Implications for Trafficability and Construction,” *Planetary and Space Science*, Vol. 210, 2025, pp. 105467, Accessed 2025-12-12.
- [86] Qian, C. et al., “The Influence of the Particle Size Distribution on SL-Manufactured Alumina Ceramics,” *Ceramics International*, Vol. 48, No. 15, 2022, pp. 2022–2036, Accessed 2025-12-10.
- [87] IntoCeramics, “Ceramic Materials & The Role of Powder Particle Size,” 2024, Blog post, accessed 2025-12-10.
- [88] “BZVSS-502 Vibratory Sieve Shaker,” Accessed 2025-12-12.
- [89] “RETSCH AS 400 Control Horizontal Sieve Shaker,” Product page for the AS 400 control horizontal sieve shaker, accessed 2025-12-12.

- [90] Shulman, H. et al., “Microwave Sintering for Lunar Base Construction,” Tech. rep., NASA Technical Reports Server, 2023, NASA overview of microwave sintering for lunar infrastructure.
- [91] Meredith, R. J. et al., “Spatial control of microwave heating using phased array antennas,” *IEEE Transactions on Microwave Theory and Techniques*, Vol. 57, No. 12, 2009, pp. 3100–3108, Demonstrates spatially controlled microwave heating using phased-array antennas.
- [92] Hagness, S. C. et al., “Near-field focusing of microwave energy using phased arrays,” *IEEE Antennas and Propagation Magazine*, Vol. 42, No. 2, 2000, pp. 20–30, Describes near-field focusing techniques for localized microwave energy deposition.
- [93] Kato, K. and Shirai, T., “Multi-step thermal design of microwave vacuum heating to basaltic regolith simulant towards lunar base construction,” *Scientific Reports*, Vol. 14, 2024, pp. 28231.
- [94] ZwickRoell, “ZwickRoell delivers one of the largest drop weight testers in the world to Gövert GmbH in Essen, Germany,” ZwickRoell Case Studies Website, 2025.
- [95] SSHL Machinery, “How Much Force Can a Hydraulic Press Produce?” SSHL Machinery Website, 2025, Published 05 May 2025.
- [96] National Aeronautics and Space Administration (NASA), “ArcJet-Complex,” NASA Ames Research Center Website, 2025, Updated 11 Dec. 2025.
- [97] Miranda, F. A., Nessel, J. A., Romanofsky, R. R., and Acosta, R. J., “A Review of Antenna Technologies for Future NASA Exploration Missions,” Tech. rep., NASA Glenn Research Center, 2006.
- [98] European Space Agency, “Communicating from Space: Gaining a Grip on Antennas,” European Space Agency, 2025.
- [99] NASA, “Communications – Hubble Space Telescope Observatory Design,” <https://science.nasa.gov/mission/hubble/observatory/design/design-communications/>, n.d., Accessed 10 Dec. 2025.
- [100] Airbus, “Airbus’s Space Technology Gets to Mars with Perseverance,” <https://www.airbus.com/en/newsroom/news/2020-07-airbuss-space-technology-gets-to-mars-with-perseverance>, Jul 2020.
- [101] Silicon Laboratories, “WGM160P Wi-Fi® Module Data Sheet,” 2025.
- [102] McCoy Components, “What Is Antenna Gain,” <https://components.mccoy.com.sg/blog/mccoy-components-18/what-is-antenna-gain-665>, 2022.
- [103] Dunmore Aerospace, “Aluminized Kapton® Film & Aluminized Polyimide Film,” <https://www.dunmore.com/products/aluminized-polyimide-film.html>, 2025.
- [104] Finckenor, M. M. and Dooling, D., “Multilayer Insulation Material Guidelines,” NASA Technical Publication NASA/TP-1999-209263, NASA Marshall Space Flight Center, 1999.
- [105] NASA Glenn Research Center, “Aerogel Reinforced Composites (LEW-TOPS-141),” <https://technology.nasa.gov/patent/LEW-TOPS-141>, n.d.
- [106] Thermtest, Inc., “A Brief Overview of Multilayered Insulation and Its Role in Protecting Spaceships and for the Extreme Temperatures in Space,” <https://thermtest.com/a-brief-overview-of-multilayered-insulation-and-its-role-in-protecting-spaceships-and-for-the-extreme-temperatures-in-space>, Feb 2022.

- [107] Sobra, K. and Branco, J. M., “Experimental evaluation of a dovetail joint,” *COST Action FP1101 Workshop*, edited by B. Franke and S. Franke, Bern University of Applied Sciences, Institute for Timber Construction, Structures and Architecture, Biel, Switzerland, September 23–24 2014, pp. 35–41, Includes papers on reliability, assessment, monitoring and strengthening of timber structures.